

# A Novel approach to portfolio construction

T. Di Matteo<sup>1,2,3</sup>, L. Riso<sup>\* 4</sup>, and M.G. Zoia<sup>4</sup>

<sup>1</sup>Department of Mathematics, King's College London, The Strand, London, WC2R 2LS, United Kingdom.

<sup>2</sup>Complexity Science Hub Vienna, Josefstadtstraße 39, 1080 Vienna, Austria.

<sup>3</sup>Centro Ricerche Enrico Fermi, Via Panisperna 89A, Rome, 00184, Italy

<sup>4</sup>Department of Economic Policy, Università Cattolica del Sacro Cuore, Milan, Italy

February 4, 2026

## Abstract

This paper proposes a machine learning-based framework for asset selection and portfolio construction, referred to as the Best-Path Algorithm Sparse Graphical Model (BPASGM). The method extends the Best-Path Algorithm (BPA) by transforming dependency discovery into a structured and economically motivated asset-selection procedure. BPASGM identifies linear and non-linear dependencies among a large set of financial assets and represents them through a sparse graphical model satisfying a structural Markov property. Building on this representation, BPASGM systematically filters out assets that are positively or redundantly connected, isolating subsets of assets that are either conditionally independent or negatively correlated. This screening step is explicitly designed to enhance diversification and to mitigate estimation error in high-dimensional portfolio problems. Portfolio construction is then performed on the selected subset by using standard mean-variance techniques. BPASGM is not intended to improve upon the theoretical mean-variance optimum under known population parameters. Rather, it aims to improve realized portfolio performance in finite samples, where classical sample-based Markowitz implementations are known to be highly sensitive to estimation error. Monte Carlo simulations show that BPASGM-based portfolios exhibit more stable risk-return characteristics, lower realized volatility, and improved risk-adjusted performance relative to standard sample-based mean-variance portfolios. An empirical application to U.S. equities, global stock indices, and foreign exchange rates over the period 1990–2025 confirms these findings and highlights the substantial reduction in portfolio cardinality achieved by the method. Overall, BPASGM provides a statistically grounded and computationally efficient framework that bridges sparse graphical modeling and portfolio theory, and represents a significant methodological extension of the original BPA for dependence-aware portfolio construction.

**Keywords:** Asset selection; Portfolio optimization; Efficient frontier; Sparse graphical models; Machine learning; BPASGM.

**JEL Classification:** C63 – Computational Techniques; Simulation Modeling; G11 – Portfolio Choice; Investment Decisions; G17 – Financial Forecasting and Simulation; C58 – Financial Econometrics; C61 – Optimization Techniques; Programming Models; Dynamic Analysis.

## 1 Introduction

Portfolio selection lies at the core of modern finance and represents one of the most enduring and intensively studied problems in investment theory. Since the pioneering work of [Markowitz \[1952b\]](#), the mean-variance framework has provided the canonical foundation for optimal portfolio construction, formalizing the trade-off between expected return and risk through the optimization of asset weights. Despite its conceptual elegance and enduring influence, the practical implementation of mean-variance optimization remains challenging. Portfolio outcomes are highly sensitive to the estimation of expected returns and,

---

\*Corresponding author. Email: luigi.riso@unicatt.it

in particular, to the estimation and inversion of the covariance matrix. Even relatively small estimation errors can lead to large variations in optimal portfolio weights [Braga et al., 2025], unstable allocations, and poor out-of-sample performance [Michaud and Michaud, 2007, Olmo, 2023]. These difficulties are exacerbated in high-dimensional settings, where the number of assets is large relative to the available time-series observations.

Over the past decades, a substantial body of literature has sought to mitigate these limitations by improving the statistical robustness of portfolio inputs or by modifying the optimization procedure itself. Prominent approaches include shrinkage estimators of the covariance matrix [Ledoit and Wolf, 2003a,b], robust and resampling-based portfolio methods [Michaud and Michaud, 2007, Martin et al., 2010, Gregory et al., 2011], Bayesian frameworks such as the Black–Litterman model [Black and Litterman, 1992], and sparse or penalized portfolio formulations [Broadie, 1993, Lefebvre et al., 2020]. While these methods can substantially improve numerical stability, they remain fundamentally dependent on the estimation of second moments and, in many cases, on the inversion or spectral decomposition of large covariance matrices. As a result, they continue to face challenges in the presence of complex dependence structures, limited sample sizes, and noisy data.

In parallel, several extensions of the efficient frontier have been proposed to reduce overfitting and improve portfolio robustness [Markowitz et al., 1999, Hakem, 2025]. These approaches often rely on restricting the investment universe, imposing additional constraints on portfolio weights, or incorporating regularization techniques to stabilize estimation.

Empirical evidence from both simulation studies and backtesting exercises suggests that such robustness-enhanced frontiers can outperform the classical Markowitz frontier in finite samples, achieving higher realized returns for a given level of risk or lower realized risk for a given return target [Bodnar et al., 2022, Zhou, 2024]. Importantly, these improvements should be interpreted as finite-sample robustness gains rather than as violations of the fundamental risk–return trade-off that characterizes the population mean–variance frontier.

A key and often underemphasized source of fragility in portfolio construction lies in the asset selection process itself. The quality of estimated returns, covariances, and risk measures depends critically on the composition of the asset universe. Including redundant assets, assets driven by similar latent sources of risk, or assets that contribute little incremental diversification can magnify estimation error and degrade portfolio performance. Improving asset selection is therefore an integral component of robust portfolio construction, as it directly affects the conditioning of the estimation problem and the stability of the resulting efficient frontier.

Methods for asset selection vary widely depending on investment objectives, data availability, and investor preferences. Existing approaches include return-oriented selection strategies [Tu and Li, 2024, Lassance and Vrins, 2023], risk-minimization criteria [Campbell et al., 2001, Fabozzi et al., 2008], and screening procedures based on environmental, social, and governance (ESG) considerations [Garcia-Bernabeu et al., 2024, Müller and Joubrel, 2025].

More broadly, asset selection techniques range from theory-driven optimization and factor-based screening to heuristic rules and discretionary or active management strategies [Brown and Smith, 2011, Carroll et al., 2017, Jacobs et al., 2014]. In practice, hybrid approaches that combine multiple criteria are often employed. Quantitative asset selection occupies a central position within this landscape.

Quantitative methods rely on econometric models, statistical techniques, and computational algorithms to rank or score assets based on observable characteristics.

Commonly used factors include valuation measures such as price-to-earnings ratios [Block, 1995, Ramadan, 2009], price-to-book ratios [Nezlobin et al., 2016], enterprise value multiples [Mauboussin, 2018, Olbert, 2025], momentum indicators, quality measures, and risk metrics such as volatility, beta, and drawdowns.

Unlike discretionary strategies, quantitative approaches are explicitly data-driven and aim to reduce subjective judgment in asset selection. In recent years, the rapid growth of high-dimensional financial datasets and advances in computational methods have fostered increasing interest in machine learning techniques for asset selection and portfolio construction [Mirete-Ferrer et al., 2022].

Many machine learning approaches focus on return prediction, feature extraction, or factor discovery [Barfuss et al., 2016, Raddant and Di Matteo, 2023]. However, comparatively less attention has been devoted to the explicit modeling of inter-asset dependence structures, which play a central role in diversification and risk management. In particular, understanding how assets are conditionally related to one another—beyond simple pairwise correlations—is crucial for identifying redundancy and improving portfolio robustness.

This paper proposes a novel methodology that directly addresses this gap. Specifically, we introduce the

*Best-Path Algorithm Sparse Graphical Model* (BPASGM), a dependence-aware framework for asset selection that integrates ideas from information theory, graphical modeling, and machine learning. BPASGM extends the Best-Path Algorithm (BPA) originally proposed by [Riso et al. \[2023\]](#).

Graphical models provide a principled way to represent complex dependency structures among random variables, with nodes corresponding to variables and edges encoding conditional dependence relationships [[Lauritzen and Wermuth, 1989](#), [Jordan et al., 2004](#)].

In high-dimensional environments, sparsity is essential, as the number of potential interrelations grows quadratically with the number of variables [[Barfuss et al., 2016](#)]. Sparse graphical models such as the Graphical Lasso [[Friedman et al., 2008](#)], Bayesian regularization approaches [[Gan et al., 2019](#)], and related methods have been widely applied in fields ranging from genetics and climate science to finance [[Bleik, 2013](#), [Zerenner et al., 2014](#), [Aste and Di Matteo, 2017](#), [Aste et al., 2010](#), [Musmeci et al., 2014](#)]. In financial applications, these models enhance interpretability and mitigate computational challenges associated with large covariance matrices. However, many existing approaches rely on precision-matrix estimation, are restricted to linear dependence, and assess relationships primarily at the pairwise level. BPASGM differs from these approaches in several important respects. First, it does not rely on the inversion or eigen-decomposition of the covariance matrix as an optimization object. Second, it allows for both linear and nonlinear dependence by leveraging information-theoretic measures. Third, it constructs a directed acyclic graphical representation that satisfies a conditional independence (Markov-type) property by design. By identifying, for each asset, a minimal set of predictors that jointly explain its behavior, BPASGM systematically prunes redundant or positively connected assets and isolates subsets of assets that are either conditionally independent or negatively related. It is important to emphasize that BPASGM is not proposed as an alternative preference model, nor as a replacement for mean–variance optimization. Rather, it should be understood as a preprocessing and screening tool that reshapes the asset universe prior to portfolio In population settings in which the true mean vector and covariance matrix are known, restricting the asset universe cannot improve upon the theoretical Markowitz optimum under the same quadratic utility, since no estimation problem is present and a smaller feasible set cannot dominate a larger one. However, BPASGM does not operate in this oracle environment, nor does it solve the same sample mean–variance problem with a reduced feasible set and fixed estimates. Instead, BPASGM introduces a data-dependent screening step that reshapes the estimation problem itself: assets are selected based on their dependence structure, portfolio moments are re-estimated on the selected subset, and mean–variance optimization is subsequently carried out using these selection-conditioned estimates. By excluding redundant and positively dependent assets and re-estimating portfolio moments on a subset with more favorable dependence properties, BPASGM reduces effective dimensionality, improves the conditioning of moment estimators, and enhances the stability and robustness of realized portfolio outcomes out of sample, without overturning the fundamental risk–return trade-off.

Monte Carlo simulations and empirical applications presented in this paper demonstrate that portfolios constructed after BPASGM-based asset selection exhibit improved diversification properties, more stable realized Sharpe and Sortino ratios, and reduced sensitivity to estimation error relative to portfolios constructed from the full asset universe. Apparent features such as locally negative realized risk–return slopes should therefore be interpreted as finite-sample robustness effects rather than as evidence of theoretical dominance or preference reversal. Moreover, BPASGM naturally leads to a substantial reduction in portfolio cardinality, yielding simpler, more interpretable portfolios without imposing ad hoc sparsity constraints on portfolio weights. The contribution of this paper is both methodological and practical. Methodologically, it introduces a dependence-aware asset selection framework grounded in graphical modeling and information theory. Practically, it provides a computationally efficient and modular tool that can be combined with standard mean–variance optimization or alternative portfolio objectives that account for downside risk or higher moments. The remainder of the paper is organized as follows. Section 2 describes the BPASGM methodology and its theoretical properties, including the conditional independence structure induced by the algorithm. Section 3 presents Monte Carlo simulations illustrating the construction of efficient frontiers based on BPASGM-selected assets. Section 4 introduces the metrics used to evaluate diversification and volatility properties of the resulting portfolios. Section 5 reports empirical results based on U.S. equities, global stock indices, and exchange rates, including out-of-sample comparisons and robustness checks. Section 6 concludes and discusses implications and directions for future research.

## 2 Best Path Algorithm for Sparse Graphical Models

### 2.1 Overview of the BPASGM procedure and its extension over BPA

BPASGM is designed as a two-stage procedure. In the first stage, a dependence-aware screening procedure is applied to a large universe of assets to identify the underlying dependence structure among them. This step relies on graphical and information-theoretic tools to characterize conditional and signed relationships among asset returns, yielding a sparse directed representation of dependence. Assets that are strongly redundant or positively dependent according to this structure are excluded, resulting in a reduced subset of assets with more favorable dependence properties. Importantly, this screening step reshapes the asset universe itself and does not involve portfolio optimization.

The second stage consists of constructing portfolio weights on the selected subset using a standard mean-variance criterion. Expected returns and covariances are re-estimated on the reduced asset set, and portfolio weights are obtained by solving a classical mean-variance optimization problem subject to the same feasibility constraints used throughout the paper. Thus, BPASGM does not modify investor preferences or the portfolio objective; it modifies the estimation problem by conditioning it on a data-driven selection of assets.

This distinction is crucial for interpreting the results of the paper. BPASGM does not aim to improve upon the theoretical Markowitz optimum defined under known population moments, nor does it correspond to solving the same sample mean-variance problem on a reduced feasible set with fixed estimates. Instead, the screening step alters the statistical properties of the estimators used in portfolio construction by reducing dimensionality and conditioning on the observed dependence structure. As a result, the relevant comparison is between portfolios constructed under different estimation problems, rather than between identical optimization problems with different feasible sets.

The strong reduction in the asset universe observed in the first stage is consistent with the presence of a low-dimensional dependence structure, a feature commonly exploited by factor models to regularize covariance estimation. However, BPASGM differs fundamentally from factor-based approaches. While factor models impose a global linear structure to stabilize the covariance matrix while retaining the full asset universe, BPASGM performs data-driven, dependence-aware asset selection, explicitly exploiting conditional and signed relationships to identify and remove redundant sources of common variation. In this sense, BPASGM reshapes the asset universe prior to optimization rather than merely regularizing second-moment estimates. To distinguish these effects empirically, the paper includes a comparison with factor-based covariance benchmarks evaluated under the same rolling out-of-sample protocol.

BPASGM also extends the original BPA in a substantive way. The BPA, as introduced in [Riso et al. \[2023\]](#), is a node-wise procedure that identifies, for a given target variable, a minimal subset of predictors that jointly explain its behavior according to an information-theoretic criterion. A natural extension is to apply BPA symmetrically to each asset in the universe, yielding a directed graph of predictive relationships. While this symmetric application is a necessary step, it is not sufficient for portfolio construction. In particular, the resulting graph may contain dense clusters of assets that are strongly and positively dependent, reflecting common sources of variation and leading to redundancy from a diversification perspective.

BPASGM goes beyond symmetric BPA by introducing additional mechanisms that actively exploit the detected dependence structure for asset selection. In particular, BPASGM constructs a signed graphical representation that distinguishes between positive and negative dependence relationships and introduces explicit pruning rules to break economically undesirable positive-dependence links. These rules are designed to eliminate redundant assets while retaining assets that contribute distinct sources of risk. As a result, BPASGM does not merely detect dependence relationships but uses them to reshape the asset universe in a way that is directly relevant for portfolio construction.

Finally, because portfolio moments must be estimated in finite samples, realized portfolio outcomes may differ from the theoretical properties of the population mean-variance frontier. Apparent features such as negative realized risk-return slopes should therefore be interpreted as finite-sample robustness effects rather than as violations of the classical risk-return trade-off. In this sense, BPASGM aims to improve the stability and robustness of realized portfolio performance by mitigating estimation error through dependence-aware asset selection, without altering the underlying economic principles of mean-variance portfolio theory.

Having outlined the objectives and structure of BPASGM at a high level, we now recall the key ideas underlying the Best Path Algorithm (BPA) [Riso et al. \[2023\]](#), which constitutes the fundamental building block of the proposed sparse graphical framework and whose extension and adaptation are central

to the construction of BPASGM. Consider a dataset  $\mathbf{X}$  consisting of  $n$  observations and  $p$  variables,<sup>1</sup> denoted as  $X_1, X_2, \dots, X_p$ . The BPA constructs an initial graphical representation of the relationships among the variables in  $\mathbf{X}$  [see, among others, [Edwards et al., 2010](#), [Riso and Guerzoni, 2022](#)]. Conceptually, the algorithm belongs to the Sequential Forward Search family [[Patil and Sane, 2014](#)], as it starts from an empty variable set and iteratively adds variables that act as potential determinants of a target variable, say  $X_i$ . The BPA leverages the dependency structure revealed by the algorithm of [Edwards et al. \[2010\]](#), which relies on the Akaike and Bayesian Information Criteria (AIC and BIC) to identify the maximum-likelihood tree within a High-Dimensional Mixed Graphical Model (HDGM). The optimal set of predictors—defined as the subset of variables connected to a given target variable, typically representing the response or dependent variable in the model [[Manual, 2013](#)—is identified using the concept of mutual information, which quantifies the amount of shared information between variables. Formally, for each variable  $X_i$ , we denote by  $\mathbf{X}_{ps_i}$  the optimal predictor set called the optimal path-step, that is, the subset of variables in  $\mathbf{X}$  providing the highest joint explanatory power for  $X_i$  in the information-theoretic sense. The BPA proves to be very effective in detecting variables’ relationships because it enables to address three critical issues that arise in the application of some of the most common used methods that are available for this scope. First, while a covariance estimate is used to determine the sign of dependencies, BPASGM does not rely on covariance inversion or penalized precision-matrix estimation, which are the primary sources of instability in high-dimensional portfolio problems [see, among others, [Friedman et al., 2008](#), [Riccobello et al., 2023](#), [Scheinberg et al., 2010](#)] second, it does not require the specification of an appropriate regularization parameter, which is employed in some optimization problem, such as Glasso, and last, it proves capable to detect relationships between variables that are not exclusively linear. Additional methodological details on the BPA are provided in Appendix A.

## 2.2 The Network Construction through the generalization of the BPA

The BPA algorithm can be iteratively applied to each variable of the dataset to construct a sparse graphical model (SGM) with specific properties. The SGM can be obtained as follows. Let us consider a dataset  $\mathbf{X}$  composed of  $p$  variables  $\{X_1, X_2, \dots, X_p\}$ . Applying iteratively the BPA to each of the  $p$  variables produces a mixed graph (MG), that it will be called BPASGM hereafter, which includes only arrows and arcs, that is bi-directed edges, not lines<sup>2</sup>. This result can be explained by noting that the relationships linking the variables selected by the algorithm may be either unidirectional or bidirectional. The relationship between two variables, say  $X_j$  and  $X_i$  (with  $i \neq j$ ), is unidirectional when the former explains the latter, that is  $X_j \rightarrow X_i$ , or vice-versa, that is  $X_j \leftarrow X_i$ ; while it is bidirectional when  $X_j \leftrightarrow X_i$ , that is when one variable affects the other and vice-versa.

When the BPA is applied, all the variables included in the optimal path-step  $\mathbf{X}_{ps_i}$  of  $X_i$  that have an explanatory role for the latter, exhibit a unidirectional relationship towards the latter. Graphically, this information is expressed through a set of arrows, originating from the nodes in  $\mathbf{X}_{ps_i}$  related to  $X_i$ , pointing towards the latter. Some of these relationships are actually bidirectional, because  $X_i$  can be in turn included in the best path-step of one of its predictors or when the optimal path-steps of  $X_i$  and of one of its predictors share some common variables.

In the former case the link between  $X_j$  and  $X_i$  is of direct type, while in the latter, is indirect because the link between  $X_i$  and one of its predictors occurs through some (one or more) other common predictors. It is important to note that BPASGM is not an undirected graph, in contrast to graphs relying on methods using the inverse of the covariance matrix (precision matrix) [[Friedman et al., 2008](#), [Meinshausen and Bühlmann, 2006](#)]. This issue underscores an important distinction between precision matrix-based approaches and BPASGM. Precision matrix-based methods assess dependencies—albeit restricted to linear relationships—at the local level, by performing pairwise comparisons between individual variables. By contrast, BPASGM examines both linear and nonlinear dependencies at the global level, enabling the comparison of a single variable with all others in the dataset.

Furthermore, the nodes of the BPASGM comply with the Markov property, as demonstrated in the following lemma:

**Lemma 2.1** (Markov-Properties). *Let  $X_i$  be a node of the BPASGM,  $\mathbf{X}_{ps_i}$  its optimal set of predictors and  $\mathbf{X}/\{\mathbf{X}_{ps_i}\}$  the set of all variables not included in  $\mathbf{X}_{ps_i}$*

$$\mathbf{X}/\{\mathbf{X}_{ps_i}\} : \quad \{X_j \notin \mathbf{X}_{ps_i} \quad j = 1, \dots, p\} \quad (1)$$

<sup>1</sup>where  $p$  can be either  $p > n$  or  $p < n$

<sup>2</sup>As it is well known, a mixed graph includes three types of edges represented by arrows, arcs (bi-directed edges), and lines (full lines) (see [Sadeghi and Lauritzen \[2014\]](#)). This mixed graph includes only the first two types of edges.

Then, it can be proved that the following property holds:

$$X_i \perp\!\!\!\perp \mathbf{X}/\{X_{ps_i}\} | \mathbf{X}_{ps_i} \quad (2)$$

**Proof:** See Appendix C.

This property implies that, once the optimal predictor set  $\mathbf{X}_{ps_i}$  is known, all remaining variables become conditionally independent of  $X_i$ . Such a structure is particularly meaningful in the context of complex systems, where interdependencies often arise from a limited set of dominant relationships. The BPASGM framework, by uncovering these minimal dependency structures, can therefore be applied beyond finance—to domains such as climate networks, neural systems, or macroeconomic interconnections—where identifying causal or informational pathways among numerous interacting components is essential for understanding the system's overall dynamics.

### 2.3 The detection of links via the matrix $\Theta$

Having established the structural and probabilistic foundations of the BPASGM, we now turn to its operational implementation. Specifically, we introduce a matrix-based representation that allows the detection and quantitative characterization of the links identified by the algorithm.

The results ensuing from the application of the BPASGM can be represented through a  $(p \times p)$  adjacent matrix, say  $\Theta$ , whose  $(i, j)$ -th entry is equal to one if the variable  $X_j$  belongs to the best path-step of the variable  $X_i$ , that is:

$$\theta_{j,i} = \begin{cases} 1 & \text{if } X_j \in \mathbf{X}_{ps_i}, \quad i, j = 1, \dots, p, \quad i \neq j. \\ 0 & \text{otherwise} \end{cases} \quad (3)$$

The matrix  $\Theta$  is a hollow matrix whose non-null entries, highlighting the optimal predictors for each variables of the graph, and it provides useful information about the occurrence of links between variables, and their nature direct rather than indirect.

The sum of each row of  $\Theta$ , say the  $i$ -th one, denotes how many times the  $i$ -th variable plays the role of predictor for other variables, that is how many times  $X_i$  appears in the best-path step of other variables. The sum of each column, say the  $j$ -th one, denotes the number of variables included in the best path-step of  $X_j$ .

To highlights the way of working of the BPASGM, let us provide an example based on a simple dataset composed by  $p = 7$  variables.

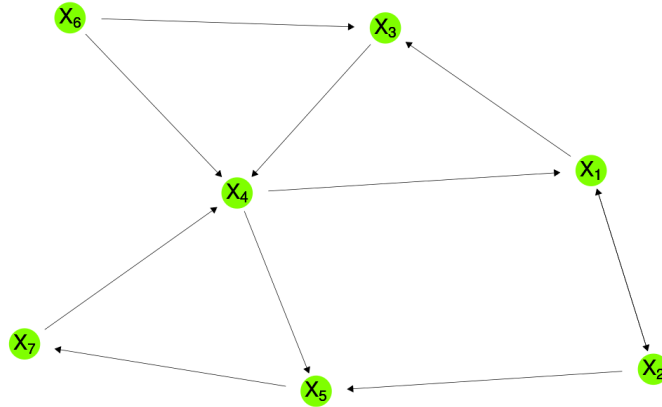


Figure 1: Example of Network build via BPASGM

The adjacent matrix for this network is

$$\Theta = \begin{bmatrix} X_1 & 0 & 1 & 1 & 0 & 0 & 0 & 0 \\ X_2 & 1 & 0 & 0 & 0 & 1 & 0 & 0 \\ X_3 & 0 & 0 & 0 & 1 & 0 & 0 & 0 \\ X_4 & 1 & 0 & 0 & 0 & 1 & 0 & 0 \\ X_5 & 0 & 0 & 0 & 0 & 0 & 0 & 1 \\ X_6 & 0 & 0 & 1 & 1 & 0 & 0 & 0 \\ X_7 & 0 & 0 & 0 & 1 & 0 & 0 & 0 \end{bmatrix}$$

Looking at the rows of this matrix, it emerges that each variable of the data set explains at most two variables. In particular,  $X_2$ ,  $X_4$ , and  $X_6$  are predictors for two other variables, while  $X_3$ ,  $X_5$  and  $X_7$  intervene in the path-step of just another variable. In particular, from the first row of this matrix it emerges that  $X_i$  is a predictor of  $X_2$  and  $X_3$ .

Looking at the columns of  $\Theta$ , it results that  $X_3$  is the variable with the highest number of predictors, three, while  $X_6$  has no predictors.

The matrix  $\Theta$  allows to determine the nature, direct, rather than indirect or simple of the links.

As explained before, a direct link between two variables occurs when each of them appears in the best path step of the other. Figure 1 highlights that a direct link exists between the variables  $X_1$  and  $X_2$

$$X_1 \leftrightarrow X_2$$

An indirect link between  $X_i$  and  $X_j$  arises when  $X_j$  appears in the optimal path step of  $X_\tau$ , and the latter, in turn, is included in the optimal path step of one or more variables that act as predictors of  $X_j$ . Thus, indirect links between two variables may occur in multiple steps, depending on the number of variables that mediate their relationship, which form a closed chain. In fact, indirect links form a closed sequence of variables in which each variable plays the role of a predictor for the one that follows in the chain.

In the network of Figure 1, examples of indirect links are

$$X_4 \rightarrow X_5 \rightarrow X_7 \rightarrow X_4, \quad X_4 \rightarrow X_1 \rightarrow X_3 \rightarrow X_4$$

Finally, a simple link between  $X_i$  and  $X_j$  occurs when  $X_j$  appears in the optimal path of one the  $X_i$  predictors, but neither direct nor indirect connections exist between  $X_j$  and  $X_i$ . In the network depicted in Figure 1, simple links are

$$X_6 \rightarrow X_4, \quad X_6 \rightarrow X_4, \quad X_3 \rightarrow X_4, \quad X_4 \rightarrow X_5, \quad X_4 \rightarrow X_1 \quad X_2 \rightarrow X_3$$

In particular it is worth noting that, while the  $i$ -th column of  $\Theta$  includes variables that play an explanatory role for  $X_i$ , its  $i$ -th row highlights which variables are explained by  $X_i$ . Thus, if one variable, say the  $X_j$  one, is simultaneously present in the  $i$ -th row of  $\Theta$  (meaning that it is explained by  $X_i$ ) and in its  $i$ -th column (meaning that it explains  $X_i$ ), a direct link occurs between  $X_i$  and  $X_j$ . This result paves the way to bring to the fore direct links between variables. In fact, direct links can be detected by computing the Hadamard product [Horn and Johnson, 2012] between the adjacent matrix and its transpose

$$D = \Theta \odot \Theta' \tag{4}$$

where  $\odot$  denotes the Hadamard product.  $D$  is a symmetric matrix, whose non-null entries highlight couples of variables directly connected. Should the  $d_{i,j}$  and  $d_{j,i}$  entries of this matrix be non-null, than a direct link between  $X_i$  and  $X_j$  occurs.

For instance, the matrix  $D$  for the example presented in Figure 1 is given by:

$$D = \begin{bmatrix} X_1 & 0 & 1 & 0 & 0 & 0 & 0 & 0 \\ X_2 & 1 & 0 & 0 & 0 & 0 & 0 & 0 \\ X_3 & 0 & 0 & 0 & 0 & 0 & 0 & 0 \\ X_4 & 0 & 0 & 0 & 0 & 0 & 0 & 0 \\ X_5 & 0 & 0 & 0 & 0 & 0 & 0 & 0 \\ X_6 & 0 & 0 & 0 & 0 & 0 & 0 & 0 \\ X_7 & 0 & 0 & 0 & 0 & 0 & 0 & 0 \end{bmatrix}$$

The simultaneous presence of not null entries in the position (1,2) and (2,1) highlights that the variables  $X_1$  and  $X_2$  are connected by a direct link, as shown in the following graph.

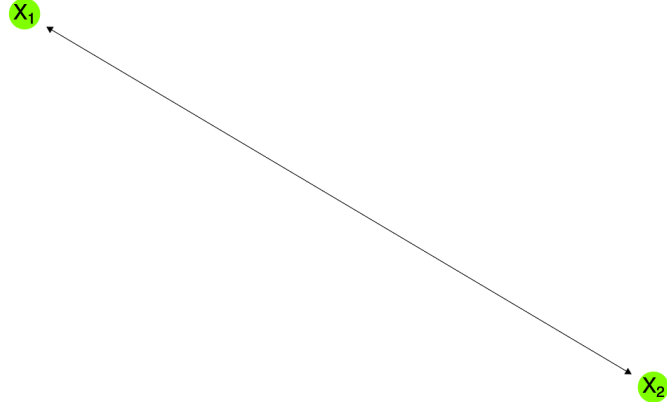


Figure 2: Representation of  $\mathbf{D}$  matrix starting from the Network in figure 1

Once the directed connections are using the matrix  $\mathbf{D}$ , indirect connections between variables can be found via the following matrix:

$$\mathbf{U} = \Theta \odot \sum_{r=2}^{p-1} ((\Theta^b)^r)' \quad (5)$$

The non-null entries of  $\mathbf{U}$  indicate couples of variables involved in closed chains. Thus, if the entries  $U_{(i,j)}$ ,  $U_{(j,\gamma)}$  and  $U_{(\gamma,i)}$  of this matrix are not null, this would mean that  $X_i$  is a predictor of  $X_j$ , which, in turn, explains  $X_\gamma$  representing a predictor of  $X_i$ , thus creating a closed chain between  $X_i$  and  $X_j$ . The following matrix  $\mathbf{U}$  represents the indirect links present in the network shown in Figure 1. The non-null entries  $u_{1,3}$ ,  $u_{3,4}$  and  $u_{4,1}$  highlight that  $X_1$  explains  $X_3$  which is in the best-path step of  $X_4$  that, in turn, is a predictor of  $X_1$ , thus forming a closed chain between these variables. Similarly, the non nullity of  $u_{7,4}$ ,  $u_{4,5}$  and  $u_{5,7}$  denote that  $X_7$  is in the best path-step of  $X_4$  which explains  $X_5$  which, in turn, is a predictor of  $X_7$ , thus forming again a closed chain. For the case under exam, both the two closed chains connect two variables,  $X_1$  with  $X_4$  the former and  $X_7$  with  $X_5$  the latter, through only a third variable,  $X_3$  and  $X_4$ , respectively.

Figure 3 represents the indirect links present in the example proposed in Figure 1

$$\mathbf{U} = \begin{array}{c} X_1 \\ X_2 \\ X_3 \\ X_4 \\ X_5 \\ X_6 \\ X_7 \end{array} \left[ \begin{array}{ccccccc} 0 & 0 & 1 & 0 & 0 & 0 & 0 \\ 0 & 0 & 0 & 0 & 0 & 0 & 0 \\ 0 & 0 & 0 & 1 & 0 & 0 & 0 \\ 1 & 0 & 0 & 0 & 1 & 0 & 0 \\ 0 & 0 & 0 & 0 & 0 & 0 & 1 \\ 0 & 0 & 0 & 0 & 0 & 0 & 0 \\ 0 & 0 & 0 & 1 & 0 & 0 & 0 \end{array} \right]$$

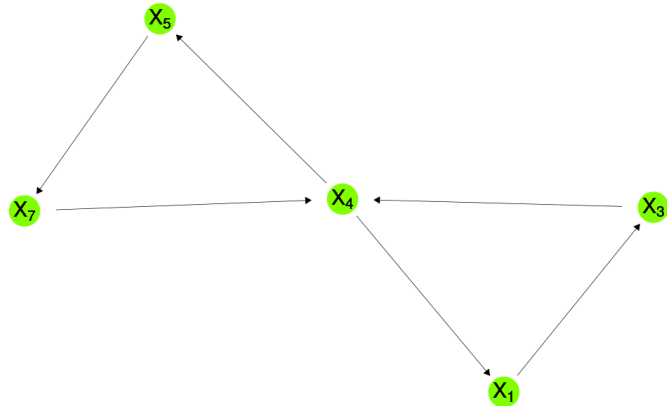


Figure 3: Representation of  $\mathbf{U}$  matrix starting from the Network in figure 1

Finally, variables can be also connected via simple or spurious links. These types of links can be detected through the following matrix

$$\mathbf{S} = \Theta - \mathbf{D} - \mathbf{U} \quad (6)$$

whose non-null entries indicate couples of variables that are connected because one explains the other but not vice versa, or indirectly, via the intermediation of one or more variables, but without forming a closed chain. The following matrix  $\mathbf{S}$  provides simple or spurious links for the network of Figure 1

$$\mathbf{S} = \begin{array}{c} X_1 \\ X_2 \\ X_3 \\ X_4 \\ X_5 \\ X_6 \\ X_7 \end{array} \left[ \begin{array}{ccccccc} 0 & 0 & 0 & 0 & 0 & 0 & 0 \\ 0 & 0 & 0 & 0 & 1 & 0 & 0 \\ 0 & 0 & 0 & 0 & 0 & 0 & 0 \\ 0 & 0 & 0 & 0 & 0 & 0 & 0 \\ 0 & 0 & 0 & 0 & 0 & 0 & 0 \\ 0 & 0 & 1 & 1 & 0 & 0 & 0 \\ 0 & 0 & 0 & 0 & 0 & 0 & 0 \end{array} \right]$$

Figure 4 shows the spurious links among the variables in the network represented in Figure 1.

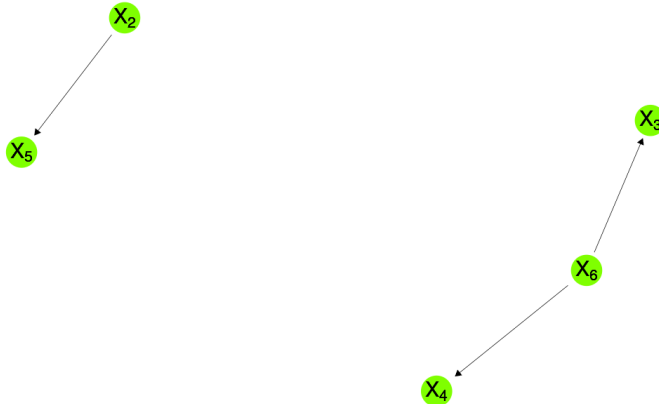


Figure 4: Representation of  $\mathbf{S}$  matrix starting from the Network in figure 1

## 2.4 From BPASGM to optimal asset selection

In the previous section, it was explained how to detect direct, indirect and simple links between variables of a given dataset through the computation of the matrices  $\Theta$ ,  $\mathbf{D}$ ,  $\mathbf{U}$  and  $\mathbf{S}$ .

In this section we use the BPASGM to construct the portfolio. In his pioneering study [Markowitz \[1952a\]](#) proved that such a portfolio should be composed of assets that are either negatively correlated or independent. The BPASGM represents a powerful tool to achieve this objective. To illustrate this, let us consider a dataset consisting of  $p$  log-returns, denoted as  $\mathbf{X}_p$ . The BPA is first applied to each variables (assets) in  $\mathbf{X}_p$ . This yields the network BPASGM. In this respect, this network effectively highlights dependencies among variables, offering valuable insights into their interconnections. Although it does not directly encode the direction (sign) of these dependencies, this aspect can be further explored through complementary analyses, which are especially meaningful in contexts such as finance. Since negatively correlated stocks are often included in a portfolio to reduce its variance, it is necessary to take into account the signed version of the adjacency matrix  $\Theta$ :

$$\Theta_s = \Theta \odot \Sigma^b \quad (7)$$

where  $\Sigma^b$  represents the positive binary form of the asset covariance matrix, defined as:  $\Sigma = \mathbb{E}[(\mathbf{X} - \boldsymbol{\mu})(\mathbf{X} - \boldsymbol{\mu})']$ <sup>3</sup>. From now on, all the matrices,  $\mathbf{D}$ ,  $\mathbf{U}$  and  $\mathbf{S}$ , which will be constructed from  $\Theta_s$ , will be denoted with the subscript  $s$ .

Then, the following three-steps procedure for constructing a portfolio that fully accounts for the asset dependencies detected by BPASGM is proposed.

<sup>3</sup>where  $\boldsymbol{\mu}$  is the mean vector of the variables in the dataset.

- **Step 1:** In the first step, an asset of interest, which serves as a starting point for constructing an appropriate portfolio, is chosen. This asset may be selected based according to its best performance across a set of  $p$  assets, as measured by standard indicators such as the Sortino ratio [Sortino and Satchell, 2001, Vinod and Reagle, 2004], the Sharpe ratio [Sharpe, 1994], or the Information Ratio [Bacon, 2023, 2021]. Alternatively, the selection of the best asset may reflect specific investor preferences. Once the initial asset is chosen, a preliminary filtering step is performed to eliminate the assets that are positively correlated to this one.

By denoting with  $j \in \{1, \dots, p\}$  the index of the selected asset, in this step all nodes that are directly linked to node  $j$ , either as source or target are eliminated.

These nodes, directly connected to node  $j$  through either outgoing or incoming edges, are highlighted by non-null entries in either the  $j$ -th row or  $j$ -th column of the binary adjacency matrix  $\Theta_s \in \{0, 1\}^{p \times p}$

$$\Theta_s = (\theta_{s,i,k})_{i,k=1}^p$$

Accordingly, the *elimination set* is given by

$$E_j = \{i \in \{1, \dots, p\} \mid \theta_{s,j,i} = 1 \vee \theta_{s,i,j} = 1\},$$

and the *reduced index set*

$$I_j = \{1, \dots, p\} \setminus E_j,$$

results to contain all indices  $i$  such that both  $\theta_{s,j,i} = 0$  and  $\theta_{s,i,j} = 0$ , i.e., all nodes that are not adjacent to node  $j$ .

The *filtered signed adjacency matrix* is the submatrix of  $\Theta_s$  indexed by  $I_j$ :

$$\tilde{\Theta}_s = (\Theta_s)_{I_j, I_j} \in \{0, 1\}^{|I_j| \times |I_j|}. \quad (8)$$

The matrix  $\tilde{\Theta}_s$  excludes all connections between asset  $j$  and the remaining nodes in the network generated via BPASGM.

At this stage, the filtered dataset is denoted as  $\mathbf{X}_z$ , where  $z < p$ . Figure 5 depicts the structure of the filtered signed adjacency matrix  $\tilde{\Theta}_s$ , obtained by considering the network illustrated in Figure 1, and assuming  $X_7$  as selected starting asset

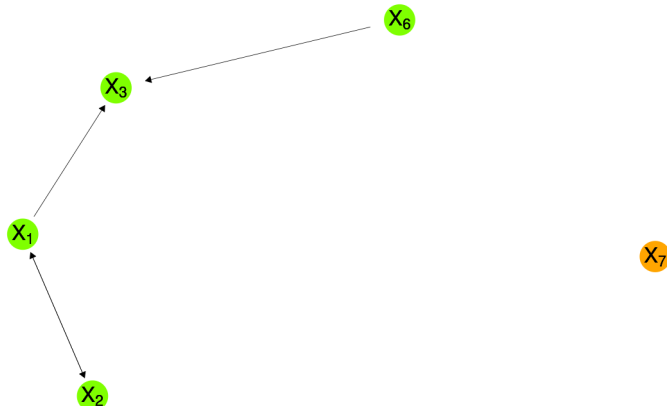


Figure 5: Representation of the signed updated matrix  $\tilde{\Theta}_s$ , resulting from Step 1, starting from the network in Figure 1, with  $X_7$  (in orange) as the selected starting asset.

- **Step 2:** From  $\Theta_s$ , the matrix  $\tilde{D}_s$ , as defined in Eq. 4, is derived. Direct (positive) links can be removed by eliminating one of the two directly connected variables using specific criteria. For instance, in each pair of variables involved in a feedback loop, one may discard the variable that appears more frequently as a predictor for other variables. Alternative criteria include eliminating the variable with the highest variance ( $\sigma_{X_j}$ ), or the one with the lowest expected return ( $\mu_{X_j}$ ). Furthermore, the selection process can be guided by performance measures such as the Sortino and Satchell [2001] index [Vinod and Reagle, 2004], the Sharpe [1994] ratio, or the Information Ratio [Bacon, 2023, 2021]. Once direct links have been removed, the signed adjacency matrix is updated.

Let  $\tilde{\Theta}_{s,u}$  denote the resulting matrix, which no longer contains direct links. At this stage, the data set is indicated by  $\mathbf{X}_k$ , where  $k < z < p$ .

The signed updated matrix  $\tilde{\Theta}_{s,u}$  resulting from the removal of the direct link between  $X_1$  and  $X_2$  in  $\tilde{\Theta}_s$  is shown in Figure 6. This matrix is obtained by using performance measures to select between the two nodes, the one ( $X_2$ ) to keep.

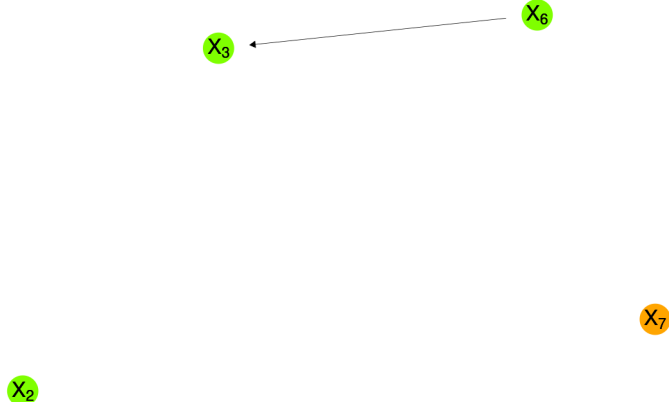


Figure 6: Representation of  $\tilde{\Theta}_{s,u}$ , resulting from Step 2, starting from the Network in figure 1 with  $X_7$  (in orange) selected starting asset

- **Step 3:** After removing direct links, the signed adjacency matrix  $\tilde{\Theta}_{s,u}$  retains only simple or undirected connections. Closed or open causal chains can be detected through the computation of the matrixes  $(\tilde{U}_{s,u})$  and  $(\tilde{S}_{s,u})$ . Then these links can be disrupted by using a criteria similar to the one previously applied to remove direct links. At this stage, the dataset is reduced to  $\mathbf{X}_h$ , where  $h < k < z < p$ . With reference to the example developed thus far, at this step only three assets remain, having removed the link from  $X_6$  to  $X_3$ , while retaining asset  $X_6$  (as shown in Figure 7).



Figure 7: Result of the **Step 3**, starting from the Network in figure 1 with  $X_7$  (in orange) selected starting asset

The remaining variables from Step 3 ( $\mathbf{X}_h$ ) no longer exhibit direct, undirected, or simple connections. However, latent dependencies can still be observed and involve only the surviving variables from Step 3 ( $\mathbf{X}_h$ ). As in previous steps, the dataset can be further refined by removing variables from  $\mathbf{X}_h$  that share a high number of common predictors or by eliminating variables that are jointly explained by a specific predictor. These refinements follow the same selection criteria outlined in previous steps. The final dataset consists of a minimal subset of assets, denoted as  $\mathbf{X}_g$ , where  $g < h < k < z < p$ , that either do not share information or share only negative dependencies. Ultimately, this procedure allows us to derive an optimal subset of variables that are either independent, thanks to the Markov property of their

network, or negatively correlated, thereby facilitating the implementation of a robust asset allocation strategy. This step of the procedure does not apply to the example considered so far, because as shown in Figure 7, the output of the first three steps is just a set of unlinked variables.

All link-removal procedures can be performed thanks to Lemma 2.1. Specifically, once the algorithm has identified the relationships among assets—reflecting the explanatory or predictive influence exerted by certain assets on others—the elimination of specific assets disrupts these dependencies. By virtue of the Markov property, such disruptions ensure the conditional independence of the remaining assets.

### 3 BPASGM at work: a simulation study

Having established the methodological foundations of BPASGM, we now turn to its simulation-based validation. This section presents a Monte Carlo study designed to assess how dependence-aware asset selection affects the realized properties of portfolios constructed under a standard mean–variance criterion in finite samples. The objective of the analysis is not to modify the Markowitz optimization problem itself, but to evaluate how a data-driven screening step that reshapes the asset universe influences the estimation of portfolio moments and the resulting portfolio outcomes.

The approach adopted in this study follows a two-stage procedure. In the first stage, BPASGM is applied to a large set of assets in order to select a subset based on their dependence structure and redundancy properties. In the second stage, expected returns and covariances are re-estimated on the selected subset, and portfolio weights are determined using the classical Markowitz mean–variance framework under the same feasibility constraints used throughout the paper. As a consequence, the portfolios considered in this section are obtained from different, selection-conditioned estimation problems rather than from the same optimization problem with a reduced feasible set and fixed estimates. The simulation results should therefore be interpreted as evidence on finite-sample robustness and stability, rather than as improvements over the theoretical Markowitz frontier defined under known population moments.

In his seminal contribution, [Markowitz \[1952b\]](#) formalized portfolio choice as a trade-off between expected return, viewed as a desirable attribute, and return variance, viewed as an undesirable one. Within this framework, an efficient portfolio maximizes expected return for a given level of risk, and the collection of all such portfolios defines the efficient frontier in mean–variance space. In the absence of a risk-free asset, this frontier corresponds to the upper branch of a hyperbola, often referred to as the Markowitz bullet. In practice, when portfolio moments are estimated from finite samples, the realized position of portfolios relative to this theoretical frontier may be substantially affected by estimation error, dimensionality, and the dependence structure among assets. These effects are particularly pronounced in high-dimensional settings, where redundancy and strong positive dependence can lead to unstable estimates and poor out-of-sample performance.

The geometry of the efficient frontier is closely linked to the correlation structure of asset returns. Negative correlations enhance diversification by shifting the frontier leftward, thereby reducing risk for a given level of expected return or increasing expected return for a given level of risk. When assets are statistically independent, diversification benefits persist, although they arise solely from the distribution of portfolio weights rather than from offsetting co-movements. As the number of independent assets increases, portfolio variance decreases with the squared portfolio weights, but these gains are generally smaller than those obtained in the presence of negative dependence. While correlation patterns play an important role in diversification, the effects documented below arise primarily from the interaction between dependence-aware asset selection and the subsequent re-estimation of portfolio moments, rather than from correlation structure alone.

Following the approach of [Broadie \[1993\]](#), we assess the effectiveness of BPASGM through controlled simulation experiments that allow us to examine how dependence-aware screening influences the realized efficient frontiers obtained under finite-sample estimation. In particular, we analyze how the selection of assets based on their dependence structure affects portfolio stability and diversification properties when standard mean–variance optimization is applied to re-estimated moments.

In this simulation study, a set of twelve artificial financial return series is generated to emulate complex dependence structures and noise characteristics commonly observed in financial markets. The simulation spans  $t = 2520$  observations for each asset, corresponding approximately to ten years of daily data assuming 252 trading days per year. Details of the data-generating process are provided in Appendix D. Figure 8 illustrates the dependence structure underlying the data-generating process, which serves as the starting point for the application of BPASGM. Building on the minimal BIC tree proposed by [Edwards et al. \[2010\]](#), the BPA is applied symmetrically to each variable, resulting in the BPASGM network shown in Figure 9. Although the data-generating process includes both linear and nonlinear dependencies, the

BPASGM network successfully captures the underlying structure among variables. Since BPASGM is here applied to financial returns, a signed adjacency matrix  $\Theta_s$  is employed, in which variables linked by negative dependencies are treated as independent in order to avoid excluding assets with diversification potential arising from negative relationships.

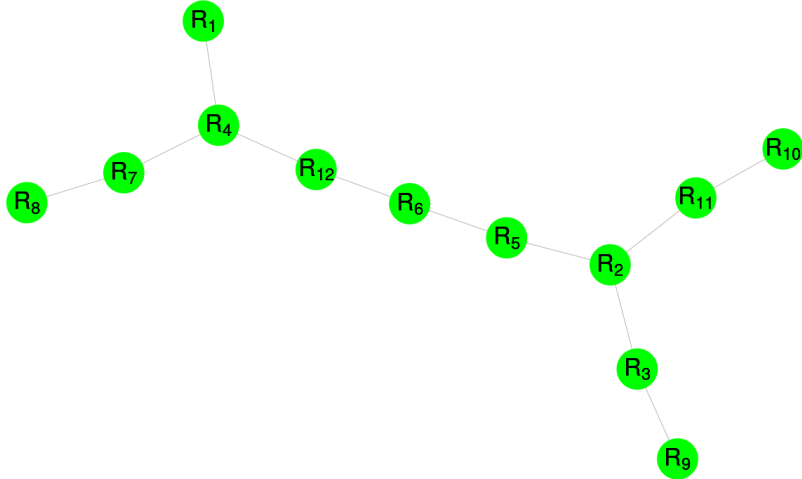


Figure 8: The minimal BIC tree of the dataset of the simulated returns  $\mathbf{X}_{\text{simulated}}$ .

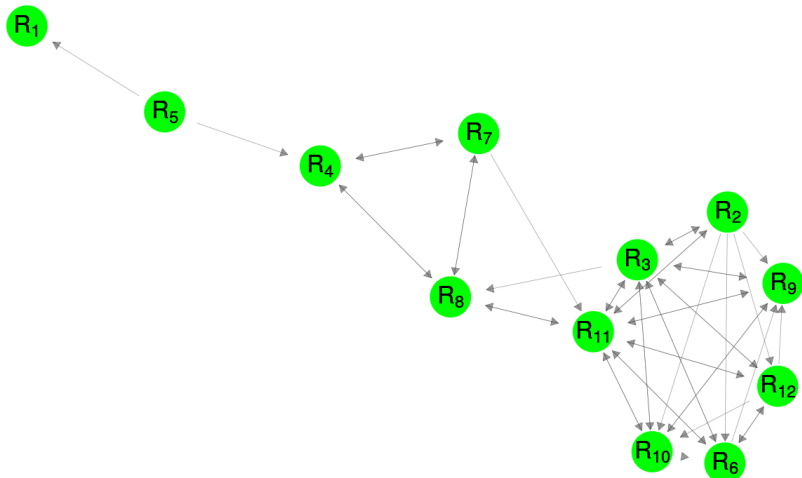


Figure 9: Representation of the matrix  $\Theta_s$  (Eq. 7) obtained through the BPASGM applied to the dataset of the simulated returns  $\mathbf{X}_{\text{simulated}}$ .

After constructing the BPASGM network, the procedure outlined in Section 2.4 is applied to derive the optimal portfolio. As previously illustrated, different approaches can be adopted to initialize the procedure, depending on the criterium used to select the starting node.

In this application, the procedure begins using as starting asset the one with the highest performance among the  $p$  simulated assets. Specifically, node  $R_{10}$  is identified as the best-performing asset according to both the Sortino and Sharpe ratios.

Then, the first Step of the procedure outlined in Section 2.4 is implemented. This involves computing the signed adjacency matrix  $\tilde{\Theta}_s$  (see Equation (8)). Figure 10a displays the updated matrix  $\tilde{\Theta}_s$ , in which all connections between asset  $R_{10}$  and the remaining nodes in the BPASGM network have been removed.

Based on  $\Theta_s$ , the matrix of direct links  $\tilde{D}_s$ , defined in Equation 4, is subsequently derived. Direct links are eliminated by removing one of the two connected assets, following a predetermined selection criterion. In the present application, the asset with the lowest Sortino ratio [Sortino and Satchell, 2001] is removed. Figure 10b illustrates the resulting matrix  $\tilde{D}_s$ .

Following Step 2 in Section 2.4, the signed adjacency matrix is then updated to exclude all direct links. The resulting matrix, denoted as  $\tilde{\Theta}_{s,u}$ , is shown in Figure 10c.

As detailed in Step 3, indirect (or undirected) connections can also be removed by applying a similar criterion, possibly adjusted to reflect investor-specific preferences. The outcome of this step is a set of completely disconnected assets, which constitutes a meaningful subset for portfolio construction. These assets are either uncorrelated or exhibit negative correlations, thereby contributing to volatility reduction. The final asset selection resulting from the BPASGM procedure is presented in Figure 10d.

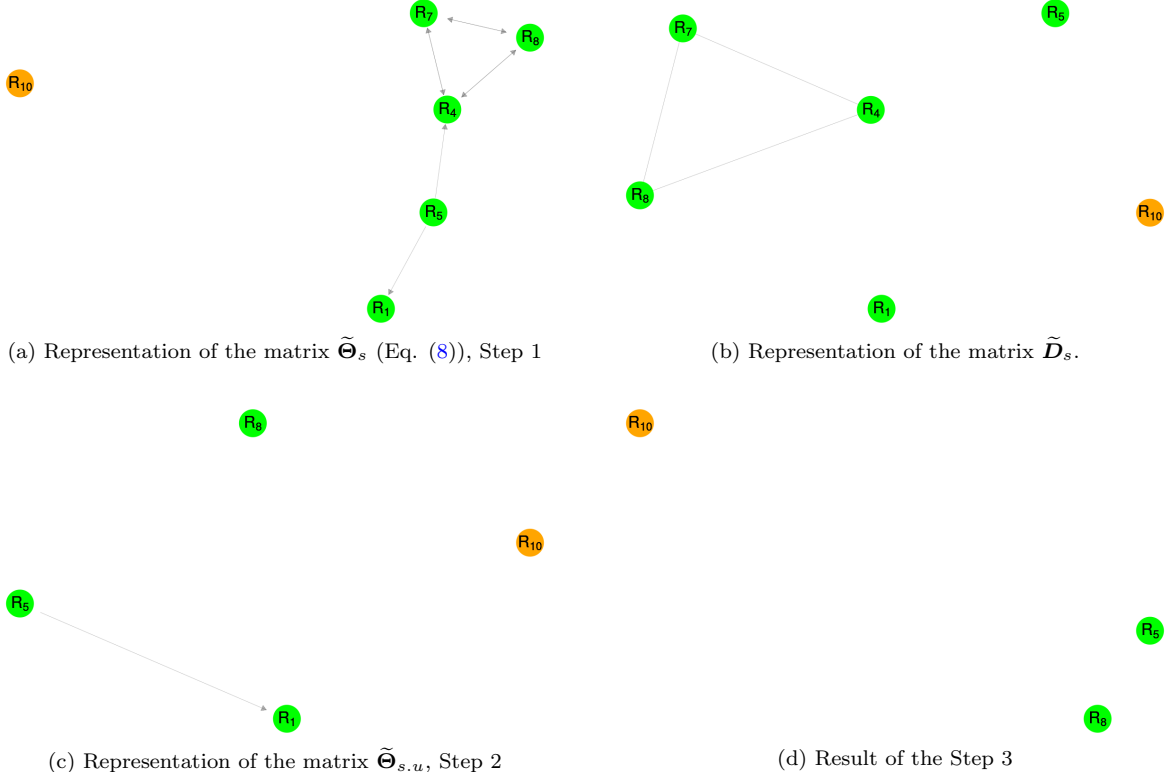


Figure 10: three-steps procedure for constructing a portfolio that fully exploits the information provided by BPASGM for the node  $R_{10}$

Figure 11 illustrates the evolution of the efficient frontier at each stage of the BPASGM-based portfolio construction procedure. The panels present a sequence of scatter plots where each grey point corresponds to a randomly generated feasible portfolio built using the returns selected at that stage by the algorithm. Red points identify portfolios on the empirical efficient frontier and the blue line represents a smoothed approximation of the frontier using a quadratic fit.

- **Panel (a):** This is the baseline scenario, displaying the feasible set of portfolios constructed from the entire dataset of simulated returns  $\mathbf{X}_{\text{simulated}}$ . The frontier is broad, indicating high diversification but also encompassing many dominated portfolios. The upper envelope (the efficient frontier) spans a wide range of risk and return.
- **Panel (b):** After applying the BPASGM procedure and selecting the assets in  $\tilde{\Theta}_s$ , the feasible set becomes more refined. The efficient frontier remains comparable to the original one in terms of shape and span, suggesting that the initial variable selection has preserved much of the portfolio efficiency.
- **Panel (c):** Once direct dependencies are removed (as encoded in  $\tilde{D}_s$ ), the feasible set contracts. The efficient frontier becomes more concave and shorter, indicating a trade-off: while some potentially profitable combinations are excluded, the selected set favors uncorrelated assets, thus improving diversification efficiency for a given level of risk.

- **Panel (d):** This final panel shows the outcome after the removal of undirected links (Step 3). The feasible set is the most constrained, reflecting the subset of fully disconnected (or negatively correlated) assets. Interestingly, although the frontier is significantly shorter, it retains a desirable shape with a smooth and well-defined curvature. This supports the idea that the BPASGM procedure succeeds in isolating a minimal yet efficient subset of assets that can still generate high-performing portfolios with reduced complexity and improved interpretability.
- More importantly, the set of portfolios located along the efficient frontier is characterized by lower risk levels and higher expected returns compared to the efficient portfolios obtained in the earlier stages of the procedure.

Overall, the progressive refinement of the asset set results in a gradual reduction of the feasible portfolio space. However, the efficient frontier remains relatively stable and well-shaped throughout, indicating that the methodology effectively filters out redundant or detrimental assets while retaining those critical for achieving optimal portfolio performance.

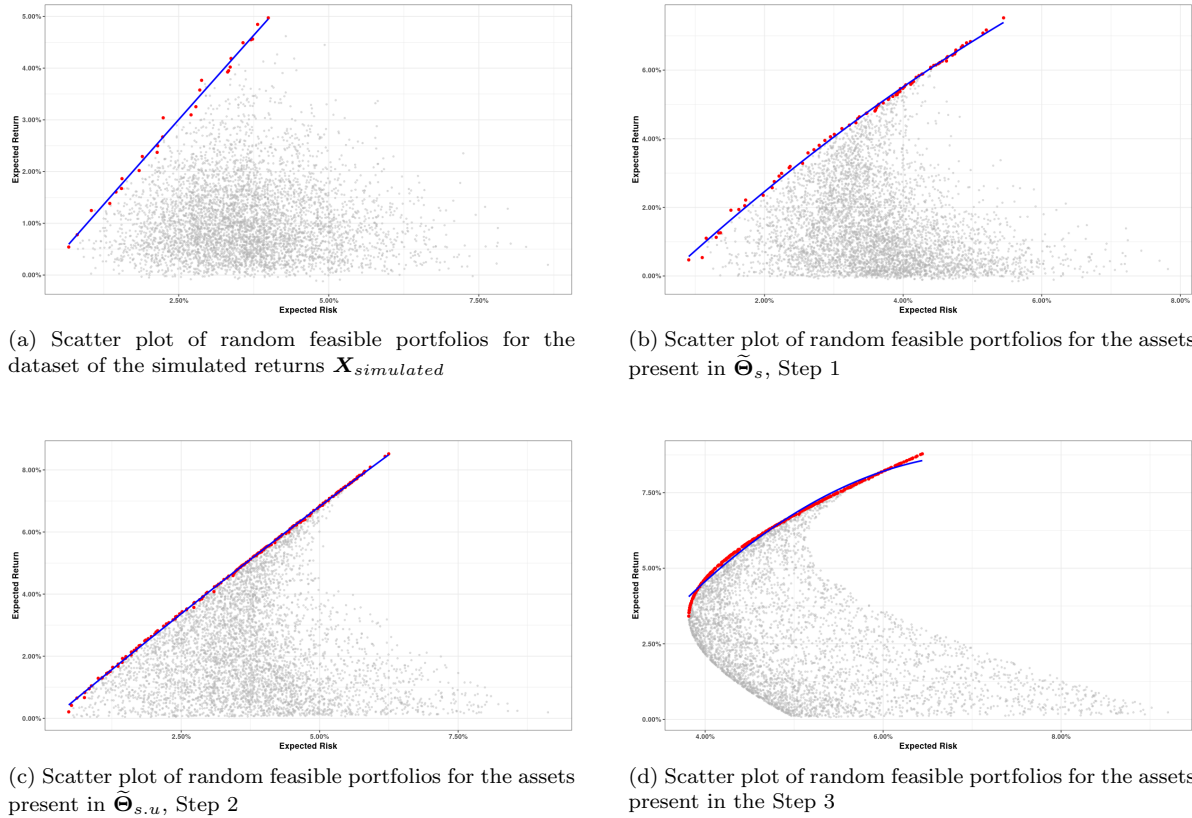


Figure 11: Efficient frontier constructed from simulated portfolios. The blue curve represents a smoothed quadratic fit over the empirical efficient frontier, derived from the set of non-dominated portfolios in the risk-return space. Grey points denote the full set of randomly generated portfolios, while red points highlight those lying on the empirical efficient frontier.

The simulation results indicate that, within this finite-sample environment, portfolios constructed after BPASGM-based asset selection exhibit more favorable realized risk–return trade-offs than portfolios obtained from uninformed asset-selection procedures evaluated under the same mean–variance criterion. These differences arise from the way BPASGM reshapes the asset universe prior to portfolio optimization, rather than from any modification of the Markowitz objective itself. To better understand the mechanisms driving these outcomes—particularly the roles of dependence structure, diversification, and estimation error—the next section provides a theoretical discussion of the statistical and structural properties of the efficient frontier.

Within this simulated environment, BPASGM systematically selects asset subsets that yield more stable and better-positioned realized portfolios relative to randomly chosen subsets of the same cardinality.

As illustrated in Figure 12, portfolios constructed from BPASGM-selected assets (red points) tend to lie above those obtained from all possible combinations<sup>4</sup> of randomly selected assets of equal size (grey points) when evaluated using selection-conditioned estimates of expected returns and covariances. This pattern indicates that BPASGM effectively exploits information embedded in the dependence structure of asset returns to avoid redundant and poorly diversified combinations that may arise under uninformed selection.

Importantly, this evidence should be interpreted as a finite-sample robustness result relative to random or uninformed asset selection, rather than as an improvement over the theoretical Markowitz frontier defined under known population moments. By conditioning the estimation of portfolio moments on a dependence-aware screening step, BPASGM reduces estimation error and improves the stability of realized portfolio outcomes without overturning the fundamental risk–return trade-off underlying mean–variance portfolio theory.

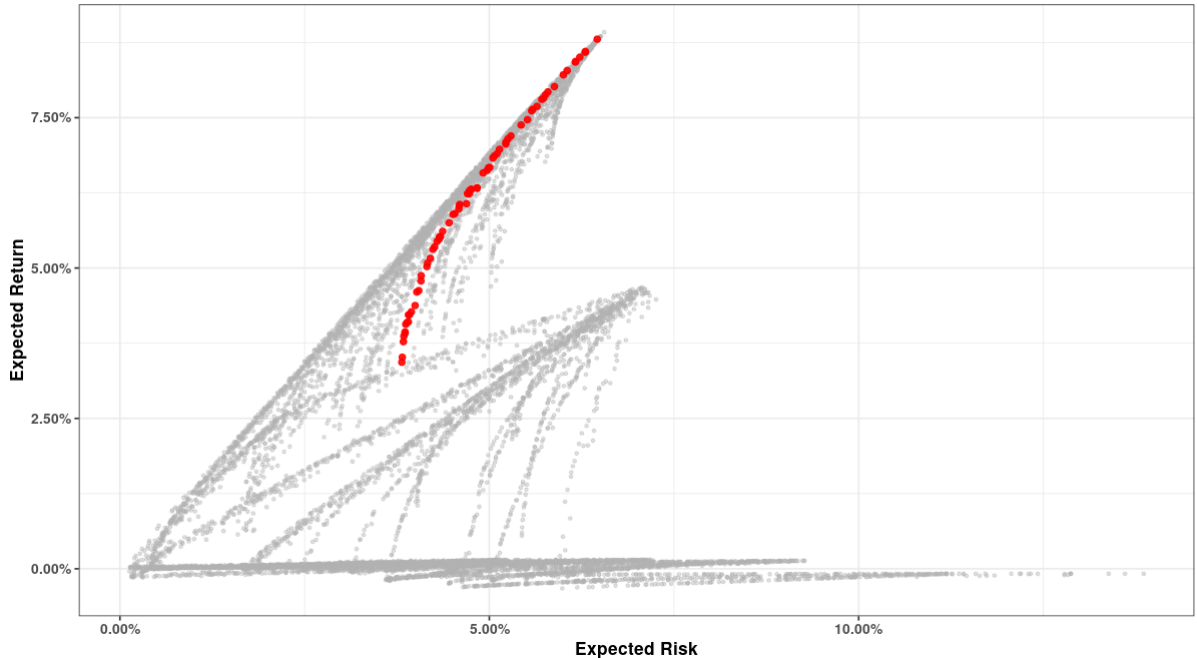


Figure 12: Efficient frontiers resulting from  $X_{\text{simulated}}$ . Grey points display all possible efficient frontiers obtained by randomly selecting the same number of assets chosen under Process 3. Red points correspond to portfolios constructed from BPASGM-selected asset subsets and illustrate the resulting realized risk–return trade-offs, which are systematically more favorable than those obtained from alternative randomly selected asset subsets of the same cardinality under finite-sample estimation.

## 4 Properties of the Efficient Frontier

Building on the Monte Carlo evidence presented in the previous section, we now examine the mechanisms through which dependence-aware asset selection influences the realized properties of portfolios constructed under a standard mean–variance criterion in finite samples. Rather than modifying the Markowitz optimization problem itself, BPASGM affects portfolio outcomes by reshaping the asset universe prior to optimization and by conditioning the estimation of portfolio moments on the selected subset. This section explores the statistical and structural features that arise from this selection process and discusses their implications for diversification and volatility dynamics.

As is well established, the shape and position of the efficient frontier depend on the statistical properties of the assets included in the portfolio and on the constraints imposed on portfolio weights. In particular, the frontier is determined by expected returns, volatilities, and correlations among assets, and is further influenced by practical considerations such as short-selling constraints and the presence or absence of a risk-free asset. When portfolio moments are estimated from finite samples, these features interact with

<sup>4</sup>We computed 220 portfolio combinations of three assets out of twelve.

estimation error and dimensionality, potentially affecting the realized performance of optimized portfolios.

Expected returns influence the vertical positioning of the frontier, while asset volatilities determine the scale of attainable risk levels. Among these determinants, the dependence structure—captured by correlations and more general forms of statistical dependence—plays a central role in shaping the curvature of the frontier. Low or negative dependence enhances diversification by allowing portfolio variance to be reduced through offsetting movements, whereas strong positive dependence limits diversification opportunities and may lead to concentrated and unstable portfolios.

The BPASGM framework is designed to exploit these mechanisms through dependence-aware asset selection. By identifying and removing assets that are strongly redundant or positively dependent, and by retaining assets that are weakly connected or exhibit negative dependence, BPASGM alters the composition of the asset universe in a way that is conducive to diversification. Importantly, this effect arises not solely from a reduction in the number of assets, but from the specific manner in which assets are selected based on their dependence structure.

In addition, BPASGM incorporates performance-based criteria, such as Sharpe and Sortino ratios, to guide the selection among directly and indirectly connected assets. This favors assets with higher expected returns or, for a given level of return, lower downside risk. As a result, when portfolio moments are re-estimated on the selected subset and standard mean-variance optimization is applied, the resulting portfolios tend to exhibit more favorable realized risk-return trade-offs in finite samples, reflecting improved diversification and reduced estimation error rather than a fundamental alteration of the theoretical efficient frontier.

In this sense, the properties discussed in this section should be interpreted as structural features induced by dependence-aware selection under finite-sample estimation, rather than as improvements over the population mean-variance frontier defined under known moments.

The remainder of this section formalizes these insights by examining how dependence-aware asset selection affects the geometry of the efficient frontier through its impact on estimated returns, variances, and dependence patterns among the selected assets.

The removal of positive dependencies and the preference for assets that are independent or negatively correlated reduce the volatility-weighted average correlation component of the Diversification Ratio, thereby increasing the ratio itself. The rise in the diversification ratio pushes the efficient frontier upward and, under certain conditions, causes the relationship between the portfolio's expected return and its volatility to become approximately linear.

To explain this intriguing result consider the diversification ratio [Meucci \[2009\]](#) which shows how diversification helps in reducing risk

$$DR = \frac{\sum_i^N w_i \sigma_i}{\sigma_p} \quad (9)$$

where  $w_i$  and  $\sigma_i$  are the portfolio weights and the volatilities of its assets and  $\sigma_p = (\mathbf{w}' \boldsymbol{\Sigma} \mathbf{w})^{1/2}$  the volatility of the portfolio. The numerator of  $DR$  is the hypothetical volatility of a portfolio with perfectly correlated assets, while the denominator is the effective volatility of the actual portfolio.

[Choueifaty et al. \[2013\]](#) provided the following decomposition of the diversification ratio:

$$DR_{\sigma_P}(\mathbf{w}) = [\rho_{MDP}(1 - CR_{MDP}) + CR_{MDP}]^{-1/2} \quad (10)$$

where  $\rho_{MDP}$  and  $CR_{MDP}$ , called volatility-weighted average correlation and volatility weighted concentration ratio respectively, are defined as follows:

$$\rho_{MDP} = \frac{\sum_{i \neq j}^N \rho_{i,j} w_i \sigma_i w_j \sigma_j}{\sum_{i \neq j}^N w_i \sigma_i w_j \sigma_j}, \quad CR_{MDP} = \frac{\sum_{i=1}^N (w_i \sigma_i)^2}{\left(\sum_{i=1}^N w_i \sigma_i\right)^2} \quad (11)$$

The weighted average correlation,  $\rho_{MDP}$ , compares the covariance of assets of the actual portfolio with that of a portfolio composed of assets perfectly correlated and it expresses the percentage risk reduction due to asset correlation. It is null when all assets are uncorrelated, while it is equal to 1 when all assets are perfectly correlated.

The weighted concentration ratio  $CR_{MDP}$  measures how concentrated are portfolio weights when adjusted by the volatility of a portfolio composed of perfectly correlated assets. Intuitively,  $CR_{MDP}$  measures the concentration of portfolio risk in a few assets. For a portfolio with equally weighted assets of similar volatilities, we have  $CR_{MDP} \approx 1/N$ , which decreases as the number of assets  $N$  increases. This implies

that the diversification gain arising from reducing concentration increases with the number of assets. In contrast,  $\rho_{MDP}$  captures the average correlation among assets and is not guaranteed to decrease as more assets are added. If the additional assets are highly correlated with the existing ones,  $\rho_{MDP}$  may remain large, limiting the diversification benefit. Consequently, the overall diversification ratio increases with the number of assets primarily through the reduction in concentration, whereas the contribution from the correlation component depends on the correlation structure of the portfolio. The BPASGM, by selecting uncorrelated or negatively correlated assets, effectively neutralizes or reduces the contribution of the  $\rho_{MDP}$  component, thereby maximizing the overall diversification ratio. Consequently, portfolios constructed using the BPASGM, having high diversification ratios, tend to exhibit lower risk for a given level of return. These portfolios push the frontier downward and to the left, achieving better risk-adjusted returns.

Essentially, BPSGM, by nullifying or reducing the role of the diversification component  $\rho_{MDP}$ , which captures the contribution of linear dependence among assets, produces maximally diversified portfolios. This allows the portfolio to reach the upper-left region of the efficient frontier, achieving a high return per unit of risk.

This property can be formally explained by noting that the portfolio's expected return can be expressed as a function of its volatility, its degree of diversification, and the average Sharpe ratio of the individual assets, as follows

$$\mu_p = \bar{s}_v DR(w) \sigma_p. \quad (12)$$

Here  $\bar{s}_v = \frac{\sum_{i=1}^N v_i s_i}{\sum_{i=1}^N v_i}$ , with  $s_i := \frac{\mu_i}{\sigma_i} \quad i = 1, \dots, N$ , denoting the Sharpe ratio of the  $i$ -th asset,  $v_i = w_i \sigma_i$ , and use of the following reformulation of the diversification ratio has been considered:

$$DR = \frac{\sum_{i=1}^N v_i \sigma_i}{\sigma_p} \quad (13)$$

where

$$\sigma_p = (\mathbf{v}' \mathbf{R} \mathbf{v}) = \left( \sum_{i=1}^N v_i \right)^2 (\rho_{MDP}(1 - CR) + CR) \quad (14)$$

with  $\mathbf{R}$  denoting the asset correlation matrix and

$$\rho_{MDP} = \frac{\rho_{i,j}}{v_i v_j} \quad i \neq j, \quad CR = \frac{\sum_{i=1}^N v_i^2}{\left( \sum_{i=1}^N v_i \right)^2} \quad (15)$$

Formula (12) highlights an additional reason underlying the shape of the efficient frontier obtained when selecting securities with the BPASGM. In fact, the algorithm selects nodes with high performance—that is, with elevated Sharpe ratios. As a result, the variability of the Sharpe ratios of the selected assets tends to be small and their mean  $\bar{s}_v$  stable. At the same time, the exclusion of correlated assets effectively eliminates the volatility weighted average correlation component  $\rho_{MDP}$ , so that the portfolio variance almost coincides with the component  $\sum_{i=1}^N v_i^2$  and the  $DR$  function varies little as the weights change. If, in particular, the mixed term includes negative elements, the portfolio variance is further reduced, flattening the frontier. The low variability of  $\bar{s}_v$  and  $DR$  therefore makes the relationship between  $\mu_p$  and  $\sigma_p$  stable and nearly linear.

The following paragraph outlines the methodologies that will be employed to verify whether the algorithm effectively selects uncorrelated assets, thereby generating an efficient frontier of portfolios characterized by stable average Sharpe ratios and consistent diversification profiles.

#### 4.1 Assessment of the characteristics of a portfolio composed of stocks selected by BPASGM.

The capability of the BPASGM approach to generate portfolios composed of low-risk, uncorrelated, or negatively uncorrelated assets can be evaluated by comparing the volatility of the resulting optimal portfolio, composed of returns selected by the algorithm, with that the same portfolio would exhibit if the assets were independent.

1. The volatility of the virtual portfolio composed of independent assets is computed as sum of the volatilities of its components determined via univariate GARCH models [Bollerslev, 1986] applied to each of its assets.
2. The volatility of the optimal portfolio resulting from the application of BPASGM, which accounts for time-varying correlations among assets, is instead evaluated via a multivariate Dynamic Conditional Correlation (DCC)-GARCH model [Engle, 2002].

The portfolio weights, required to compute the volatility of these two portfolios are determined using the global minimum variance strategy proposed by [Markowitz \[1952a\]](#).

This comparison is useful for assessing whether the volatility of the portfolio constructed using BPASGM is lower than that of a portfolio composed of independent assets. If the latter proves to be greater than the volatility of the optimal portfolio identified through BPASGM and evaluated using a DCC-GARCH model, accounting for potential asset correlations, then the asset selection performed by BPASGM can be considered effective. In fact, such a result would suggest that BPASGM implicitly selects either independent assets or assets characterized by negative correlations. Conversely, if the DCC-GARCH model reveals significant and time-varying co-movements, this would indicate that BPASGM does not efficiently select the assets within the portfolio.

The volatility of the virtual portfolio requires the implementation of univariate GARCH( $p, q$ ), for modeling the conditional variance  $\sigma_{i,t}^2$  of each return series  $r_{i,t}$ , specified as follows

$$r_{i,t} = \mu_i + \varepsilon_{i,t}, \quad \varepsilon_{i,t} = \sigma_{i,t} z_{i,t}, \quad z_{i,t} \sim \mathcal{N}(0, 1), \quad (16)$$

$$\sigma_{i,t}^2 = \gamma_i + \sum_{j=1}^p \alpha_{i,j} \varepsilon_{i,t-j}^2 + \sum_{k=1}^q \beta_{i,k} \sigma_{i,t-k}^2, \quad (17)$$

where  $\mu_i$  is the conditional mean of  $r_{i,t}$  and  $\gamma_i > 0$ ,  $\alpha_{i,j} \geq 0$  and  $\beta_{i,k} \geq 0$  are parameters that can be estimated by maximum likelihood. For each asset, the optimal GARCH order  $(p, q)$  is selected using the Bayesian Information Criterion (BIC) to balance fit and parsimony. Assuming conditional independence across assets, the portfolio variance at time  $t$  can be computed as follows

$$\sigma_{p,t}^{2,\text{uni}} = \sum_{i=1}^N w_i^2 \sigma_{i,t}^2, \quad (18)$$

where  $w_i$  denotes the portfolio weight of asset  $i$  (obtained via [Markowitz \[1952a\]](#) strategy), and  $N$  is the number of assets.

The volatility of the optimal portfolio resulting from the application of the BPASGM has been estimated via a multivariate DCC-GARCH model [Engle, 2002], which decomposes the conditional covariance matrix into individual volatilities and a time-varying correlation matrix. The model for the set of  $N$  returns  $\mathbf{r}_t = (r_{1,t}, \dots, r_{N,t})^\top$  is specified by

$$\mathbf{r}_t = \boldsymbol{\mu}_t + \boldsymbol{\varepsilon}_t, \quad \boldsymbol{\varepsilon}_t \sim \mathcal{N}(0, \mathbf{H}_t), \quad (19)$$

$$\mathbf{H}_t = \mathbf{D}_t \mathbf{R}_t \mathbf{D}_t, \quad (20)$$

where  $\boldsymbol{\mu}_t$  is the vector of the expected value of the conditional  $\mathbf{r}_t$ ,  $\mathbf{H}_t$  is the matrix of the conditional variances of  $\boldsymbol{\varepsilon}_t$  specified as in (20). Here,  $\mathbf{D}_t = \text{diag}(\sigma_{1,t}, \dots, \sigma_{N,t})$  is the diagonal matrix of the conditional standard deviation of  $\boldsymbol{\varepsilon}_t$  estimated from univariate GARCH models, applied to the assets, and  $\mathbf{R}_t$  is the conditional correlation matrix specified as follows ( [Engle \[2002\]](#) )

$$\mathbf{R}_t = \text{diag}(\mathbf{Q}_t)^{-1/2} \mathbf{Q}_t \text{diag}(\mathbf{Q}_t)^{-1/2}, \quad (21)$$

with

$$\mathbf{Q}_t = (1 - a - b) \bar{\mathbf{Q}} + a \mathbf{z}_{t-1} \mathbf{z}_{t-1}^\top + b \mathbf{Q}_{t-1}, \quad (22)$$

where  $\bar{\mathbf{Q}}$  is the unconditional covariance of the standardized residuals  $\mathbf{z}_t = \mathbf{D}_t^{-1} \boldsymbol{\varepsilon}_t$  and  $(a, b)$  are the DCC parameters satisfying  $a, b \geq 0$  and  $a + b < 1$  to guarantee that the estimated  $\mathbf{H}_t$  is positive. From a practical standpoint, the conditional correlation between assets  $i$  and  $j$  evolves dynamically as

$$\rho_{ij,t} = \frac{q_{ij,t}}{\sqrt{q_{ii,t} q_{jj,t}}}, \quad (23)$$

where  $q_{ij,t}$  is the  $(i, j)$ -th element of the matrix  $Q_t$ .

The portfolio variance estimated using a DCC-GARCH is given by:

$$\sigma_{p,t}^{2,\text{dcc}} = \mathbf{w}^\top \mathbf{H}_t \mathbf{w}, \quad (24)$$

The two portfolio volatilities  $\{\sigma_{p,t}^{\text{uni}}\}$  and  $\{\sigma_{p,t}^{\text{dcc}}\}$  are then compared. A persistently lower  $\sigma_{p,t}^{\text{dcc}}$  would indicate the presence of meaningful, time-varying negative correlations, thus confirming that BPASGM selects independent assets or assets that exhibit a negative dependence, enhancing diversification and reducing portfolio volatility.

To evaluate stepwise enhancements in portfolio performance, the Sortino and Sharpe ratios are calculated for the optimal portfolios derived from the assets identified by the algorithm at each iteration. The capability of the BPASGM to generate an efficient frontier of portfolios characterized by stable average Sharpe ratios and consistent diversification profiles can be assessed by computing the diversification ratios and its components at the different selection steps of the procedure.

This will make it possible to observe how the volatility-weighted average correlation decreases at each step, leading to an increase in the diversification ratio. In addition, at each step the mean and variance of the portfolios along the empirical frontier will be computed, and the coefficient of determination from the linear regression

$$\mu_P = \alpha + \beta \sigma_P + \epsilon \quad (25)$$

calculated. An increase in the latter from one step to the next serves as an indicator of the proportional relationship between  $\mu_P$  and  $\sigma_P$ .

Finally, the stability of the Sharpe ratio and the diversification ratio of the portfolios along the efficient frontier will also be subject to evaluation.

## 5 An Empirical Application of the BPASGM

The performance of the asset selection method proposed in this study is evaluated via an empirical application that uses returns (computed as the first-order differences of logarithmic closing prices [Pan and Liu, 2018]) of three categories of financial assets: (i) the 333 most highly capitalized stocks in the U.S. market (commonly referred to as Blue-chip stocks, which include companies such as “Microsoft” and “Apple”, and generally consist of well-established firms listed on the stock exchange prior to 1 January 1990), (ii) the 16 most prominent global stock indices (such as the “S&P 500”, “STOXX Europe 600”, and “FTSE 100”), and (iii) the 9 most frequently traded exchange rates. The dataset covers the period from 1 January 1990 to 31 December 2025. The dataset was retrieved from *Refinitiv Workspace*. Table 2 provides the identification codes of the assets used in this analysis.

### 5.1 The Network of dependencies brought to the fore by BPASGM

To assess the effectiveness of the BPASGM-based approach, outlined in Section 4.1, the dataset has been partitioned into a training and a testing set. Specifically, data from 1 January 1990 to 31 October 2024 have been used for training (dataset  $\mathbf{X}_{\text{training}}$ ), while data from 31 October 2024 to 31 December 2025 have been used for testing (dataset  $\mathbf{X}_{\text{test}}$ ). During the training phase, the BPASGM has been applied to select returns to include in the portfolio.

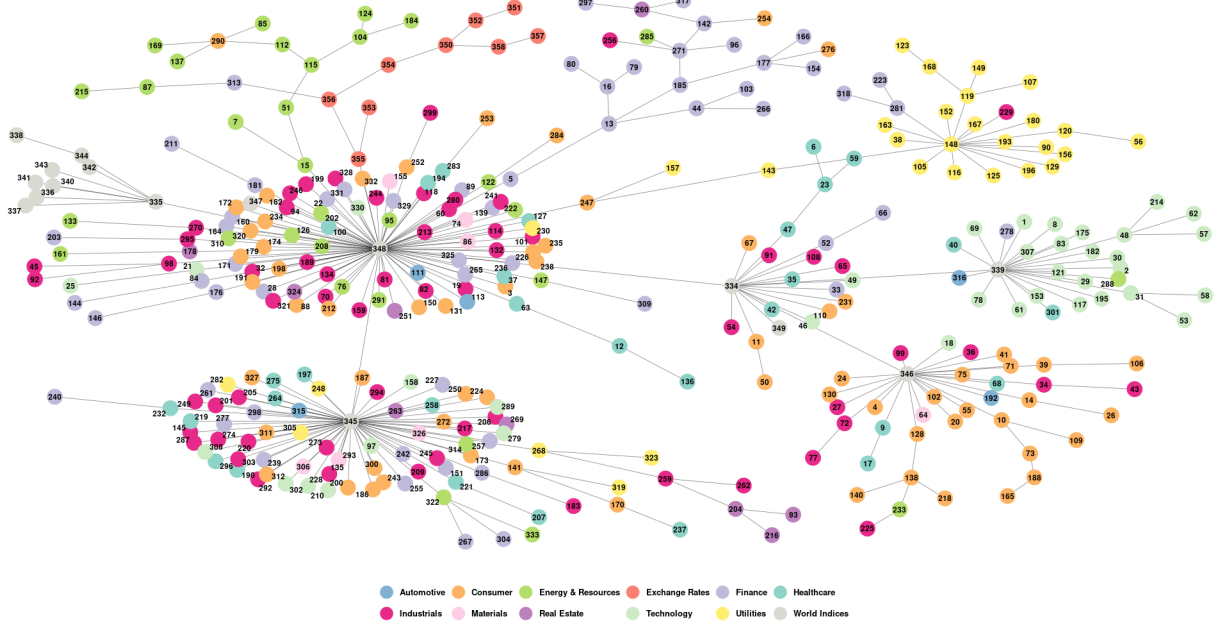


Figure 13: The minimal BIC tree of the dataset of the returns  $\mathbf{X}_{\text{training}}$ , sample period from 1 January 1990 to 30 October 2024

Figure 13 illustrates the starting point for constructing the optimal portfolio using the BPASGM-based approach. The nodes in the figure are color-coded according to the sectors to which the corresponding returns belong. Table 2 in Appendix B reports the labels of the nodes represented in the graph. Specifically, the figure illustrates the network structure underlying the variables in the dataset  $\mathbf{X}_{\text{training}}$ , as identified by the algorithm proposed by [Edwards et al. \[2010\]](#), which highlights the relationships among the returns.

It is worth noting that the structure of this high-dimensional graphical model consists of a single, large connected component, the minimal BIC tree. Within this component, distinct clusters can be identified. Some are organized around global market indices (represented by the gray nodes), while others are clearly associated with specific economic sectors. For example, there is a cluster corresponding to the *Utilities* sector (yellow nodes), another to *Energy & Resources* (light green nodes), and one composed of *Exchange rates* (dark orange nodes). In particular, the Exchange Rates cluster exhibits only a single direct connection to the financial clusters. Specifically, node 355 (“USD/CAD Exchange Rate”) is directly linked to node 348 (“NYSE Composite Index”), whereas the remaining exchange rate variables primarily display interconnections among themselves.

Within the cluster centered on global market indices, node 339 (“NASDAQ Index”) functions as a key hub for stocks in the *Technology* sector (e.g., “Microsoft”, “Apple,” and “Oracle”). Node 346 (“Dow Jones Index”) is predominantly associated with stocks in the *Consumer* and *Industrial* sectors. Nodes 348 (“NYSE Composite Index”) and 345 (“Russell 2000 Index”) operate as central hubs for heterogeneous stocks, as the nodes connected to them span multiple sectors. Finally, node 335 (“STOXX Europe 600 Price Index”) serves as a central reference point for other international indices.

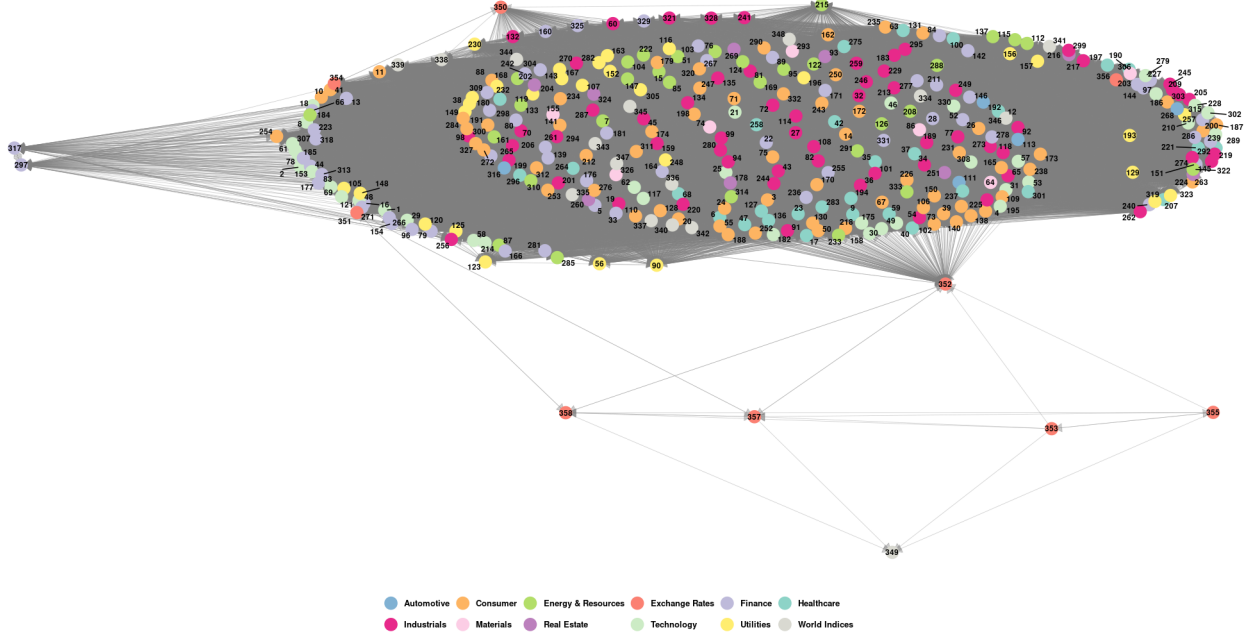


Figure 14: Representation of the matrix  $\Theta_s$  (Eq. 7) obtained through the BPASGM applied to the return dataset  $\mathbf{X}_{\text{training}}$ , over the sample period from 1 January 1990 to 30 October 2024.

Figure 14 illustrates the outcome of the iterative application of the BPA to each node in the network of the minimal BIC tree (see Figure 13). This procedure results in the BPSGM, as described in Section 2.2.

After adjusting for the negative links, which are removed so that variables connected by negative dependencies can be treated as independent, the remaining connections between variables identified by BPSGM can be used to construct the adjacency matrix  $\Theta_s$  (Equation 7)

Unlike Figure 13, which reveals distinct clusters within the network structure, Figure 14 does not clearly display any evident clusters. However, it highlights significant dependencies between almost all stocks included in the data set  $\mathbf{X}_{\text{training}}$ , with the exception of four exchange rates (nodes 353, 355, 356, and 357, respectively, corresponding to the “CAD to USD Exchange Rate 5”, “CAD to USD Exchange Rate 7”, “USD to AUD Exchange Rate”, and “HKD to USD Exchange Rate”) and node 349, which represents the “VIX index”.

It is particularly noteworthy to consider the role of the latter index, which appears detached from the core of positive dependencies represented by the main network component. Commonly referred to as the “Fear Index,” it captures market participants’ expectations of future volatility. More specifically, it reflects the implied volatility of “S&P 500” index options over a 30-day horizon and serves as a widely used proxy for the level of uncertainty or perceived market risk [Whaley, 2000].

## 5.2 Optimal asset selection

After constructing the BPASGM, the procedure described in Section 2.4 is applied to select the assets for building an optimal portfolio from a risk perspective. As outlined in the previous section, different approaches can be adopted to initialize the procedure, selecting as the starting node the asset that exhibits the best performance according to standard metrics such as the Sortino ratio [Sortino and Satchell, 2001, Vinod and Reagle, 2004] or the Sharpe ratio [Sharpe, 1994], or alternatively, an asset that reflects investor-specific preferences. For example, one might prioritize the most highly capitalized asset or the one characterized by the lowest volatility.

In this case, node 42 (“Danaher”) was selected as the starting asset, since it represents the best-performing asset according to both the [Sortino and Satchell, 2001] and Sharpe [1994] ratios. Subsequently, the adjacency matrix  $\tilde{\Theta}_s$  was computed as described in Section 2.4 (see Equation (8)).

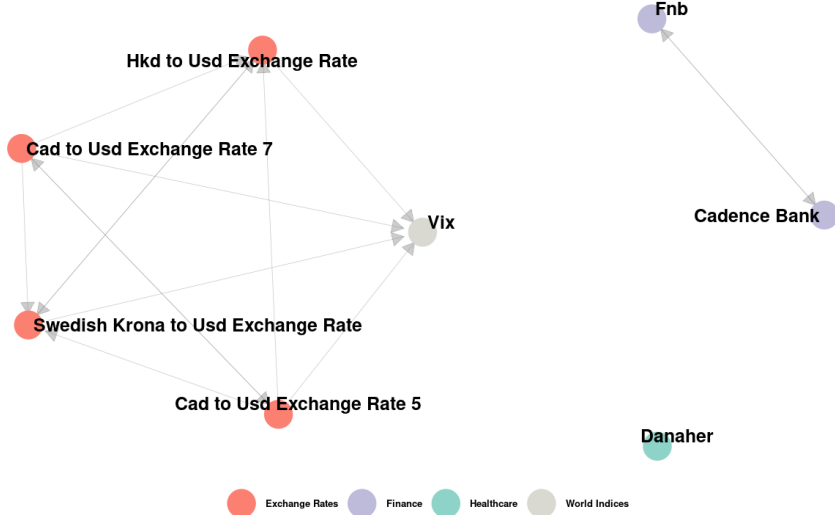


Figure 15: Representation of the matrix  $\tilde{\Theta}_s$  (Eq. (8)) obtained starting from the node 42, “Danaher”-Step 1.

Figure 15 shows the updated signed adjacency matrix,  $\tilde{\Theta}_s$ , after all connections between the asset “Danaher” and the remaining nodes in the network generated via BPASGM have been removed. It is worth noting that the elimination of all variables positively connected to the node of interest resulted in a drastic reduction in the number of variables, decreasing from 358 to 7.

The structure shown in Figure 15 preserves the dependencies between the exchange rates and the “VIX index”, as well as the bidirectional dependence between “FNB” and “Cadence Bank”.

Using  $\tilde{\Theta}_s$ , the matrix of the direct links  $\tilde{D}_s$ , as defined in Eq. 4, is derived. Direct links can be removed by eliminating one of the two connected assets according to specific criteria. In this application, the asset with the lowest performance, measured by the Sortino index [Sortino and Satchell, 2001], was removed. Notably, the final results remain unchanged when asset performance is assessed using the Sharpe ratio [Sharpe, 1994]. Figure 16 shows the matrix of direct links  $\tilde{D}_s$ .

It should be emphasized that the “VIX index” is not involved in any positive direct connections. The set of exchange rates appears divided into two distinct groups of positive direct links: on the one hand, the “CAD to USD Exchange Rate 7” and “CAD to USD Exchange Rate 5”; on the other hand, the “HKD to USD Exchange Rate” and the “SEK to USD Exchange Rate”. In addition, a positive direct link is observed between “FNB” and “Cadence Bank”. The least-performing assets, according to the [Sortino and Satchell, 2001] index, which have consequently been excluded, are “FNB”, “HKD to USD Exchange Rate”, and “CAD to USD Exchange Rate 5”.

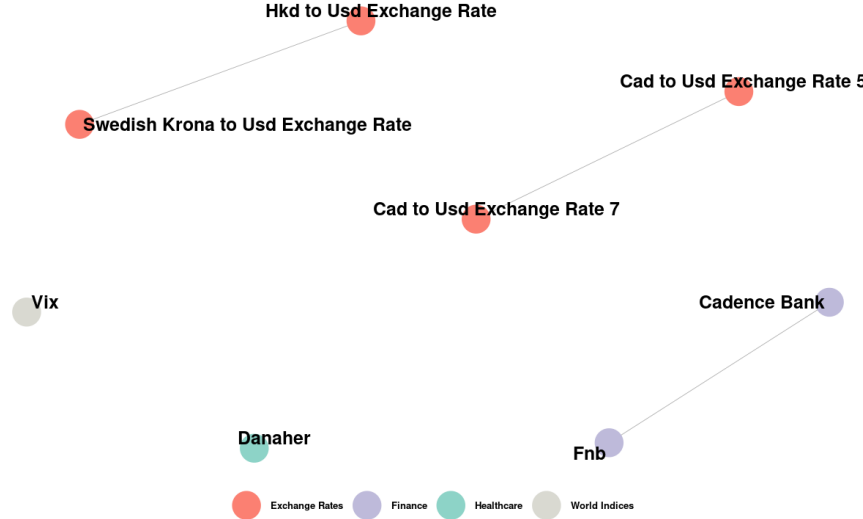


Figure 16: Representation of the matrix  $\tilde{D}_s$  obtained starting from the node 42, “Danaher”.

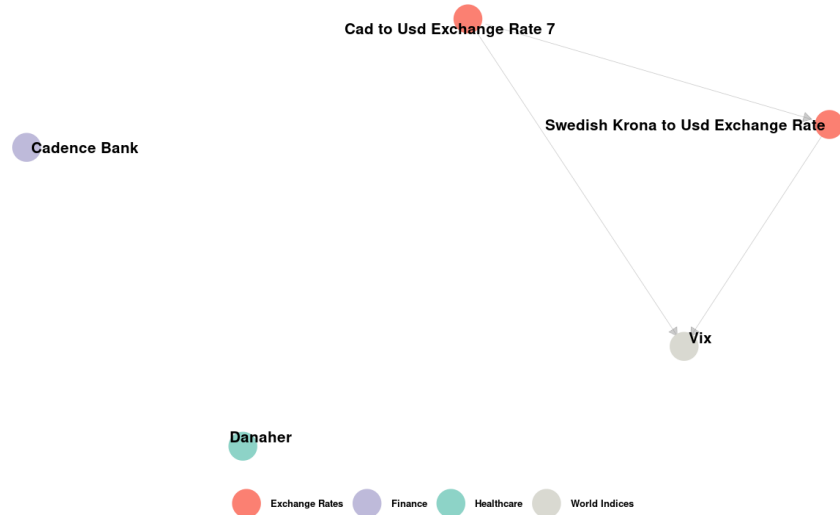


Figure 17: Representation of the matrix  $\tilde{\Theta}_{s.u}$  obtained starting from the node 42, “Danaher”-Step 2.

As reported in Step 2 of Section 2.4, once the direct links have been removed, the signed adjacency matrix is updated. Figure 17, which shows the updated matrix  $\tilde{\Theta}_{s.u}$ , highlights two isolated nodes (“Cadence Bank” and the starting node “Danaher”) as well as a cluster of nodes connected by simple links (as defined in Section 2.3), involving “VIX index”, “SEK to USD Exchange Rate”, and “CAD to USD Exchange Rate7”.

As outlined in Step 3 of Section 2.4, simple or undirected connections can be eliminated using criteria analogous to those previously applied to direct connections, taking into account specific investor’s preferences or performing measures. The outcome of this stage is a set of assets that are either unconnected or negatively correlated, and therefore suitable for constructing a portfolio with reduced volatility.

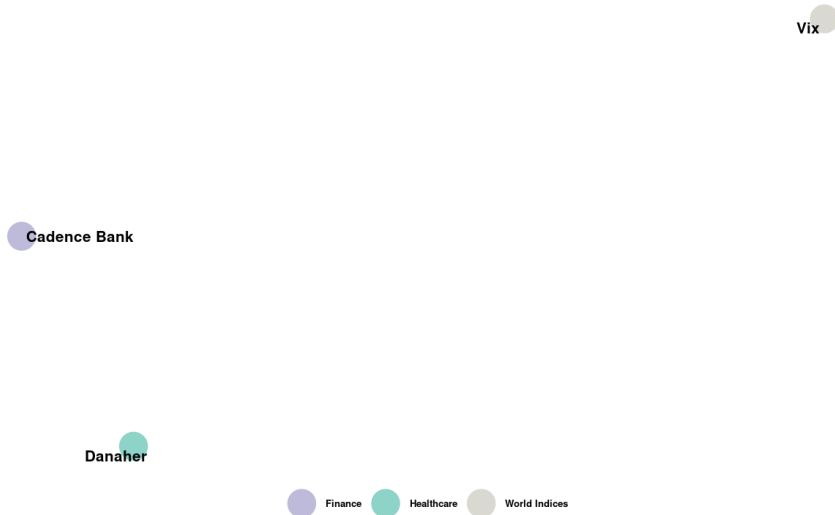


Figure 18: Result of the Step 3 starting from the node 42, "Danaher".

Figure 17 presents the final set of assets obtained at this stage. which includes, in addition to the node "Danaher", also the nodes "Cadence Bank" and the "VIX index". The following section is devoted to analyze the properties of this portfolio.

### 5.3 Properties of optimal portfolios

The properties of the optimal portfolio, resulting from the application of the BPASGM approach, are analyzed under different profiles. First, the set of all feasible portfolios that could be obtained from the returns selected by the algorithm is identified and analyzed. Subsequently, both the Sharpe ratio and the Sortino index of the optimal portfolios - built with assets weighted according to Markowitz coefficients and selected by the algorithm at the different stages of the procedure - are computed.

Furthermore, the variance of the optimal portfolio is calculated, following the approach outlined in Section 2.4. Specifically, the volatility of the optimal portfolio is estimated using a DCC-GARCH model and compared with the volatility that the same portfolios would display if its constituents were assumed to be independent.

To carry out this analysis, first a set of feasible portfolios is built, by randomly assigning weights to the assets selected by the BPSGM. This yields the scatter plot represented in Figure 19.

This figure reports the realized risk–return characteristics of the portfolios generated under the different portfolio construction procedures. The presence of regions with a negative slope in the empirical risk–return relationship should not be interpreted as a violation of the classical risk–return trade-off, nor as evidence of dominance over the theoretical mean–variance frontier. In the population setting with known moments, a risk-averse investor would rationally select portfolios on the Pareto-efficient segment of the frontier, and dominated portfolios would never be chosen.

The patterns observed in Figure 19 arise in a finite-sample environment, where portfolio moments must be estimated and are therefore affected by estimation error. In this setting, classical sample-based mean–variance optimization may lead to portfolios that are inefficient *ex post*, resulting in realized outcomes where higher returns are associated with lower realized risk. BPASGM mitigates this issue by performing dependence-aware asset selection and re-estimating portfolio moments on the selected subset, which improves the conditioning of the estimation problem and leads to more stable realized outcomes.

Accordingly, Figure 19 should be interpreted as illustrating robustness gains rather than a fundamental change in investor preferences or in the risk–return trade-off. The apparent improvements reflect BPASGM's ability to reduce estimation error and to select assets with favorable dependence properties, thereby shifting realized portfolio outcomes closer to the efficient region relative to classical sample-based mean–variance portfolios.

This pattern reflects the impact of dependence-aware asset selection on finite-sample portfolio performance. Under the specific selection criteria proposed in this study—which systematically remove redundant and positively dependent assets—it is possible to construct portfolios that exhibit more stable realized risk–return characteristics than portfolios built from the full asset universe using standard

sample-based estimation. Importantly, this does not represent a violation of the theoretical risk–return tradeoff. Rather, it demonstrates that conditioning portfolio construction on the dependence structure can substantially reduce estimation error, leading to realized outcomes that lie closer to the population-efficient frontier than those obtained under naive sample-based Markowitz optimization. This outcome is not only theoretically intriguing, but also has profound implications for asset allocation strategies and constrained portfolio optimization, as it highlights regions of the feasible portfolio mean volatility set capable of delivering superior performance.

It is important to emphasize that BPASGM does not solve the same mean–variance optimization problem on a reduced feasible set. Rather, BPASGM introduces a data-dependent screening step that conditions the estimation of portfolio moments on the selected subset of assets. Specifically, assets are first selected based on their dependence structure, after which expected returns and covariances are re-estimated on the resulting subset and mean–variance optimization is performed using these selection-conditioned estimates. As a consequence, BPASGM does not seek to improve upon the theoretical Markowitz optimum defined under known moments, nor does it correspond to restricting the feasible set under fixed estimates. Instead, it defines a different estimation problem in which dependence-aware selection and dimensionality reduction mitigate estimation error and improve the conditioning of moment estimators, thereby enhancing the stability and robustness of realized portfolio outcomes out of sample without overturning the fundamental risk–return trade-off.

Accordingly, the relevant comparison is not between

$$\max_{w \in \mathcal{W}} U(\hat{\mu}, \hat{\Sigma}) \quad \text{and} \quad \max_{w \in \mathcal{W}_g} U(\hat{\mu}, \hat{\Sigma}), \quad \mathcal{W}_g \in \mathcal{W}$$

which would mechanically favor the larger feasible set, but between two distinct optimization problems,

$$\max_{w \in \mathcal{W}} U(\hat{\mu}, \hat{\Sigma}) \quad \text{and} \quad \max_{w \in \mathcal{W}_g} U(\hat{\mu}_g, \hat{\Sigma}_g),$$

where  $(\hat{\mu}_g, \hat{\Sigma}_g)$  are the re-estimated moments after the data-driven screening step. These problems are not equivalent, as the screening procedure alters both the dimensionality and the statistical properties of the estimators used in portfolio construction.

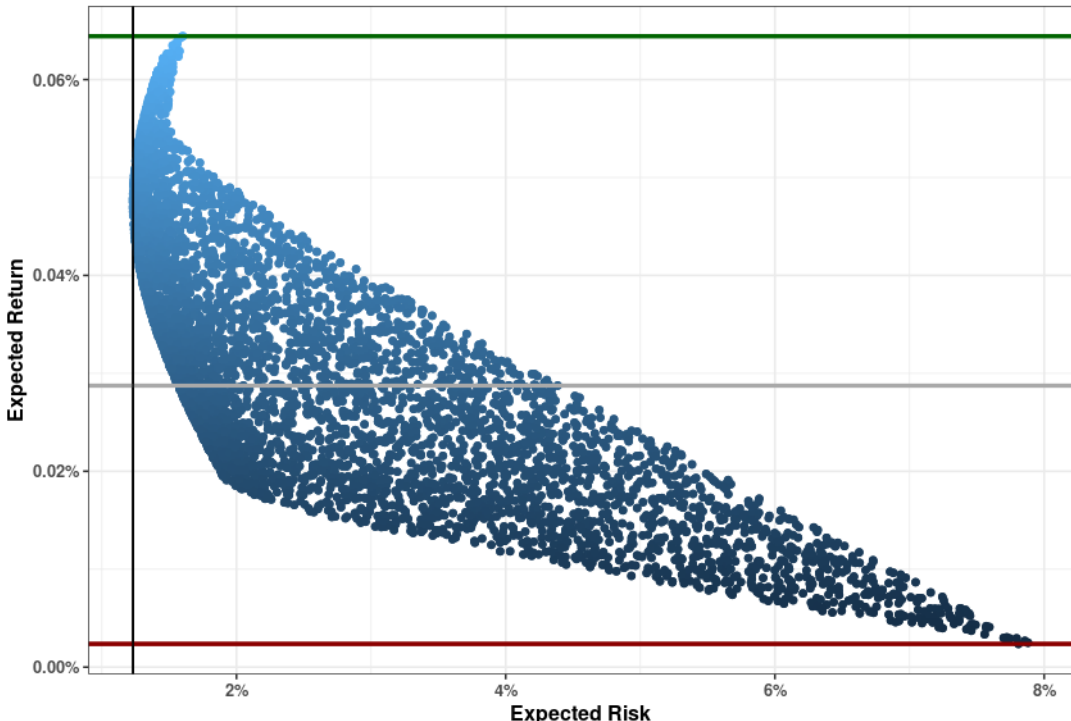


Figure 19: Scatter plot of random feasible portfolios for the assets detected by BPASGM, starting from the node “Danaher”. It shows the trade-off between portfolio risk and expected return. Horizontal lines mark the maximum (green), median (gray), and minimum (red) portfolio returns, while the vertical line denotes the portfolio with minimum risk.

Both the Sortino ratio and the Sharpe ratio are computed for the optimal portfolios constructed from the assets selected by the algorithm at each step. Asset weights are determined according to the minimum-variance strategy. Figures 20 illustrate the evolution of the annualized Sharpe ratios (panel (a), 20a) and the annualized Sortino ratios (panel (b), 20b). In both cases, the results indicate that as the algorithm progresses through its steps and the set of assets considered for inclusion in the portfolio is reduced, the financial performance of the resulting portfolios improves. This evidence confirms that an appropriate selection of independent or negatively correlated assets, as proposed in this study, enhances portfolio performance, even when the final portfolio contains a reduced number of assets.

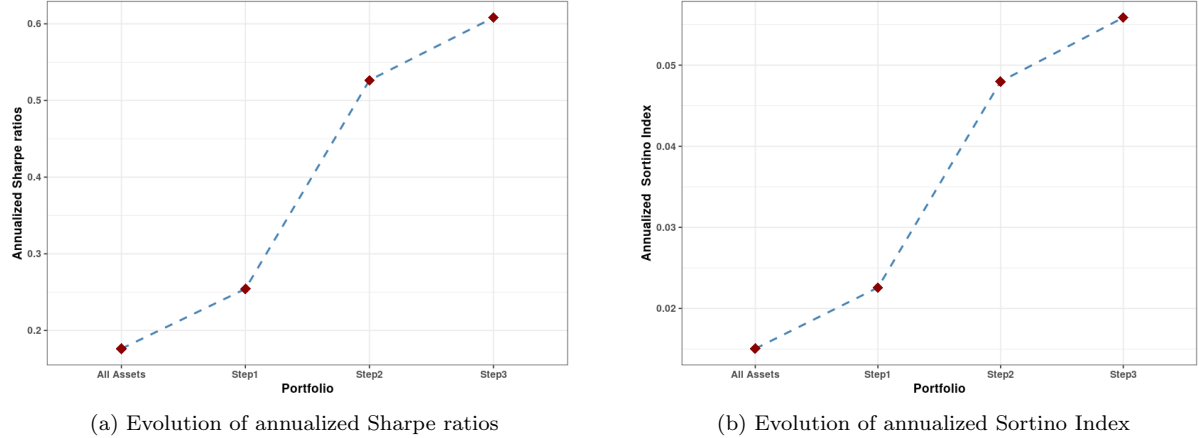


Figure 20: Annualized Sharpe ratios (panel (a)) and annualized Sortino Index (panel (b)) for each portfolio stage—“All Assets,” “Step 1”, “Step 2”, and “Step 3”— for the node “Danaher”.

At every stage, the correlation-dependent component of the diversification index, known as the weighted average correlation component  $\rho_{MDP}$ , defined in equations 10 and 11, was likewise computed. Figure 21 illustrates the evolution of  $\rho_{MDP}$  at the various steps of the BPASGM. It emerges that, as the algorithm progresses through its steps, the progressive exclusion of positively correlated assets results in a decrease in the value of  $\rho_{MDP}$  which gradually declines.

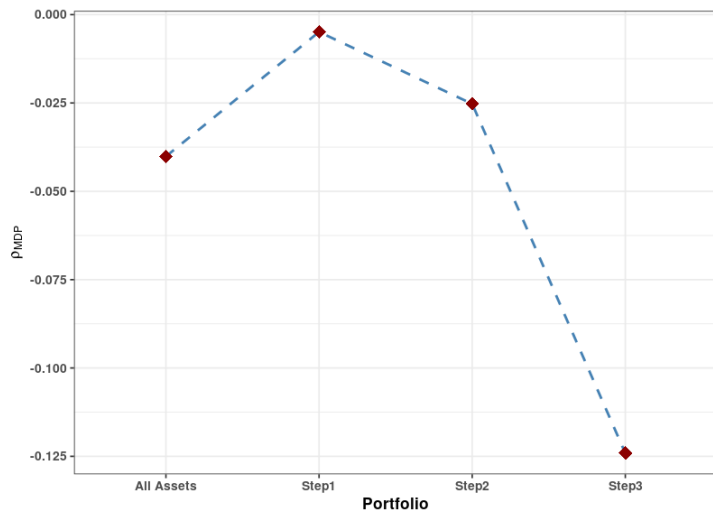


Figure 21: Evolution of  $\rho_{MDP}$  as define in equation 11 for each portfolio stage—“All Assets,” “Step1”, “Step2”, and “Step 3”— for the node “Danaher”.

In addition, to examine the existence of an inverse relationship between the mean returns and volatilities of the optimal portfolios composed of stocks selected by BPASGM, the coefficients of the regressions

specified in (25) were estimated. Table 1 presents the regression results for the optimal portfolios constructed from the stocks selected by the BPASGM at the successive stages of the algorithm. At the initial stage, portfolios are formed from the full universe of assets, while in the subsequent stages only the assets progressively selected by the BPASGM. Each column reports the estimated intercept ( $\hat{\alpha}$ ) and slope ( $\hat{\beta}$ ), together with their standard errors, significance levels, and the adjusted coefficient of determination ( $\bar{R}^2$ ). When all assets are included,  $\hat{\beta}$  is positive and highly significant, consistent with the classical positive relationship between risk and expected return predicted by portfolio theory. As the algorithm progresses, however,  $\hat{\beta}$  turns negative while remaining statistically significant. This shift indicates that, as redundant or weakly contributing assets are progressively filtered out, the conventional risk–return trade-off is reversed: portfolios with lower volatility begin to exhibit higher excess returns. In the final selection step (Step 3),  $\hat{\beta}$  becomes strongly negative, underscoring the dominance of diversification effects over the traditional linear risk–return mechanism. At the same time, the adjusted  $\bar{R}^2$  rises sharply—from low values in the early stages to  $\bar{R}^2 = 0.596$  in the final selection—signaling a substantial increase in explanatory power and the emergence of a more stable and well-defined empirical frontier.

Overall, these results demonstrate that the BPASGM procedure constructs efficient frontiers characterized by increasingly negative risk–return slopes but higher explanatory power at each step. The monotonic increase in  $\bar{R}^2$ , combined with the progressively more negative  $\hat{\beta}$ , suggests that as redundant assets are eliminated, the BPASGM isolates a subset of portfolios where diversification effects systematically dominate the traditional risk premium, leading to a structurally inverse risk–return relationship. This progressive improvement in explanatory power and the simultaneous strengthening of the inverse risk–return coefficient are consistent with Lemma 2.1, which theoretically underpins the algorithm’s selection mechanism. Specifically, once the BPASGM identifies the dependency structure among assets—capturing the explanatory or predictive influence that certain assets exert on others—the elimination of selected assets disrupts these dependencies. By virtue of the Markov property, such disruptions enforce conditional independence among the remaining assets, thereby refining the informational structure of the portfolio and amplifying its explanatory coherence, as empirically reflected in the increasing  $\bar{R}^2$  and the growing magnitude of  $\hat{\beta}$ .

This supports the interpretation that the procedure enhances diversification and reduces redundancy, producing portfolios with more stable performance profiles, as illustrated in Figures 20 and 21. Figures 22 reflect these results; the 5,000 portfolio samples are the gray points, while the red points identify the portfolios on the efficient empirical frontier, and the blue line represents a smoothed approximation of the frontier using a quadratic fit.

The performance of the optimal portfolio obtained via BPASGM is compared with that of the GLASSO technique in Appendix E. For completeness, Appendix E reports a comparison between BPASGM-based portfolios and portfolios constructed using covariance matrices estimated via the graphical lasso (Glasso). This comparison highlights a fundamental methodological distinction. Glasso enforces sparsity directly at the level of the inverse covariance matrix by imposing an  $\ell_1$  penalty, thereby regularizing second-moment estimation while retaining the full asset universe. In contrast, BPASGM does not aim to estimate a sparse precision matrix. Instead, it performs dependence-aware asset selection that reshapes the asset universe prior to portfolio optimization, after which portfolio moments are re-estimated on the selected subset.

The results reported in the appendix indicate that while sparse covariance regularization can mitigate estimation error, it does not fully address redundancy arising from strongly dependent assets when the full universe is retained. BPASGM complements these approaches by explicitly removing redundant assets rather than only shrinking their dependence structure. As a consequence, differences in performance should be interpreted as arising from fundamentally different mechanisms—asset selection versus covariance regularization—rather than from alternative tuning of the same estimation problem.

Table 1: Linear regressions of portfolio returns along the empirical efficient frontier on portfolio volatility (Eq. (25)) for different selection steps of the BPASGM procedure — for the node “Danaher”.

	<i>Dependent variable: <math>\mu_p</math></i>			
	<b>All Assets</b>	<b>Step 1</b>	<b>Step 2</b>	<b>Step 3</b>
$\hat{\beta}$	0.008*** (5.611e-04)	-0.002*** (1.399e-04)	-0.003*** (1.166e-04)	-0.007*** (7.864e-05)
$\hat{\alpha}$	0.0002*** (5.936e-06)	0.0002*** (1.892e-06)	0.0002*** (2.418e-06)	0.0005*** (2.515e-06)
Observations	5,000	5,000	5,000	5,000
$\bar{R}^2$	0.043	0.027	0.108	0.596

*Note:*

\*p<0.1; \*\*p<0.05; \*\*\*p<0.01

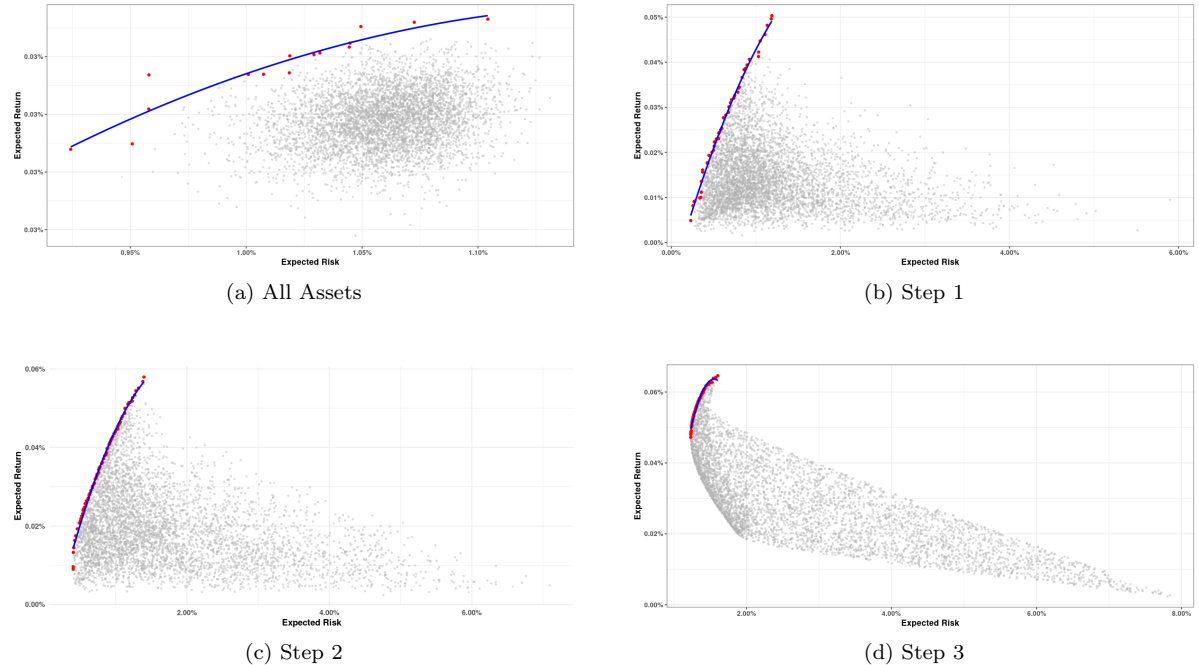


Figure 22: Efficient frontier constructed from the dataset, applying the BPASGM procedure initialized at the “Danaher” node. The blue curve represents a smoothed quadratic fit of the empirical efficient frontier, derived from the set of non-dominated portfolios in the risk–return space. Grey points denote the complete set of randomly generated portfolios, while red points highlight those located on the empirical efficient frontier.

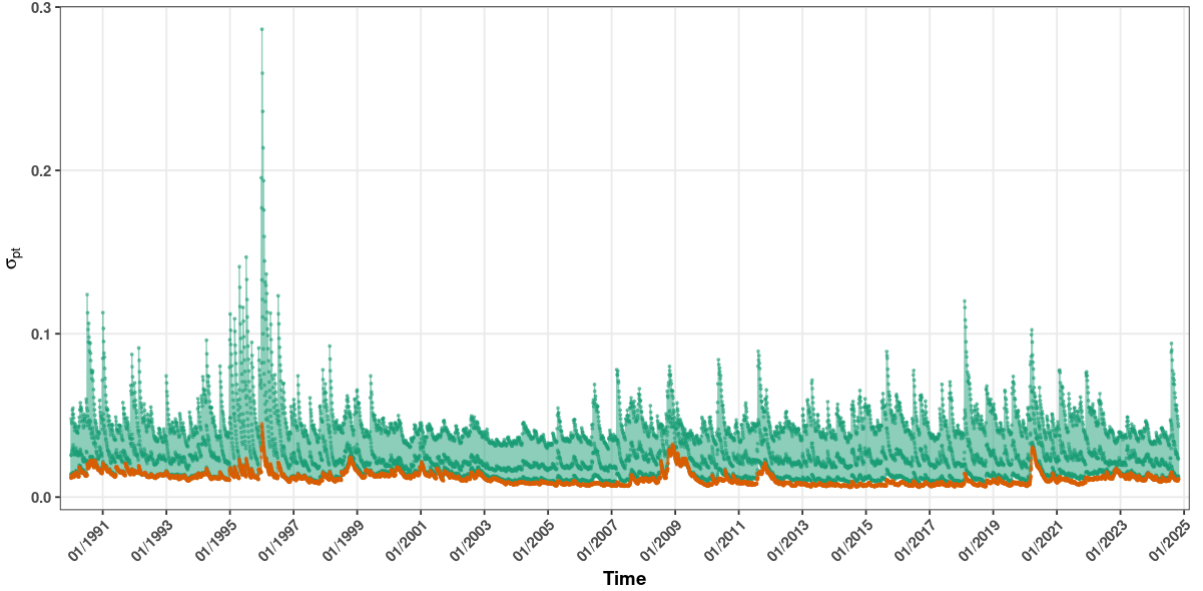


Figure 23: In-sample volatility trajectories estimated by the univariate GARCH model (green) and the DCC-GARCH model (orange) for the optimal portfolio starting from the node “Danaher”.

Finally, Figure 23 presents the in-sample volatility trajectories: the green line represents estimates from univariate GARCH models applied to the individual assets—weighted by the Markowitz coefficients—that compose the optimal portfolio, while the orange line corresponds to the DCC-GARCH model applied to the optimal portfolio originating from the ‘Danaher’ node. The figure reveals that, while both models capture common periods of heightened market volatility—such as the mid-1990s and the 2008 financial crisis—the DCC-GARCH model consistently produces lower and smoother volatility estimates compared to the univariate GARCH specification.

This discrepancy is particularly meaningful, as it highlights that the multivariate DCC-GARCH model better exploits diversification benefits. By incorporating dynamic (negative) conditional correlations, the model accounts for time-varying interdependencies and cross-asset risk spillovers, resulting in a dampening effect on overall portfolio volatility. In contrast, the univariate GARCHs, that model each asset independently, fail to capture these diversification effects and, consequently, overestimates aggregate volatility.

These findings provide empirical support for the theoretical framework outlined in Section 4.1, demonstrating that portfolios constructed using BPASGM—which incorporates time-varying negative correlations—exhibit lower overall volatility compared to portfolios in which assets are simply independent. The Figures 24 illustrate the time-varying conditional correlations  $\rho_t$  (Eq. (23)) estimated using a DCC-GARCH model over the in-sample period for the optimal portfolio originating from the node “Danaher”. As shown, the  $\rho_t$  between the “VIX” index and “Cadence Bank” (24a), as well as the  $\rho_t$  between the “VIX” index and “Danaher” (24b), are consistently negative throughout the period. In contrast, the  $\rho_t$  between “Cadence Bank” and “Danaher” (24c) exhibits more variability, with fluctuations and spikes in both positive and negative directions.

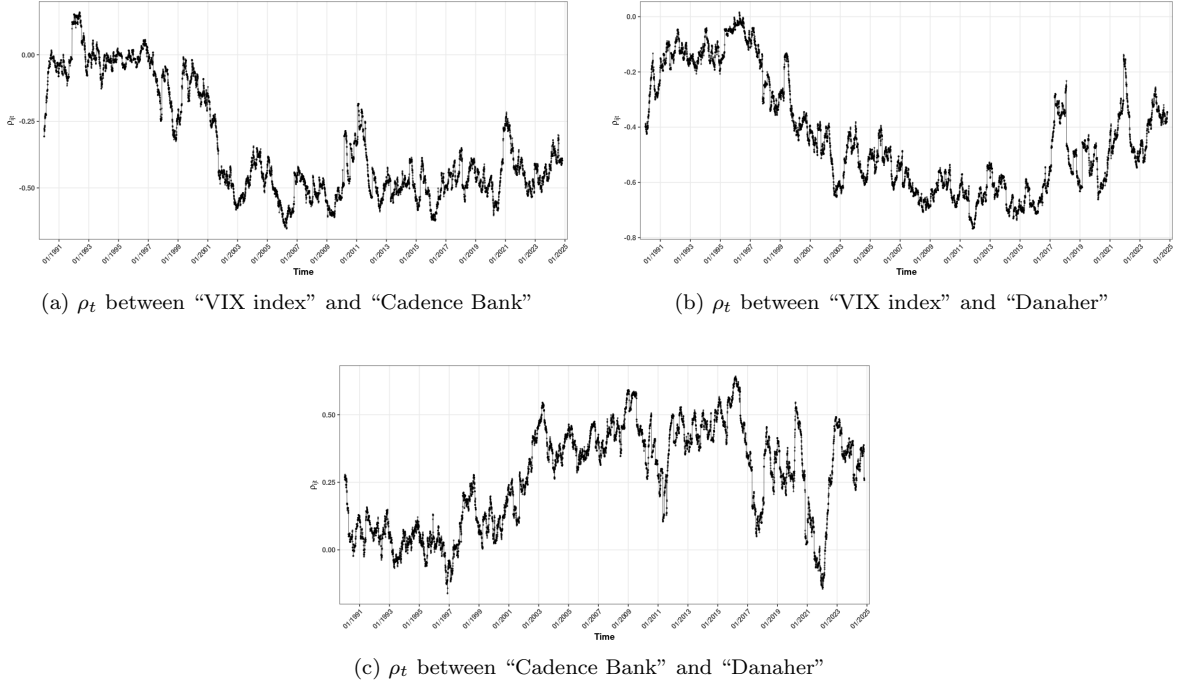


Figure 24: Time-varying conditional correlations  $\rho_t$  (Eq. (23)) estimated via a DCC-GARCH model for in-sample period for the optimal portfolio starting from the node “Danaher”.

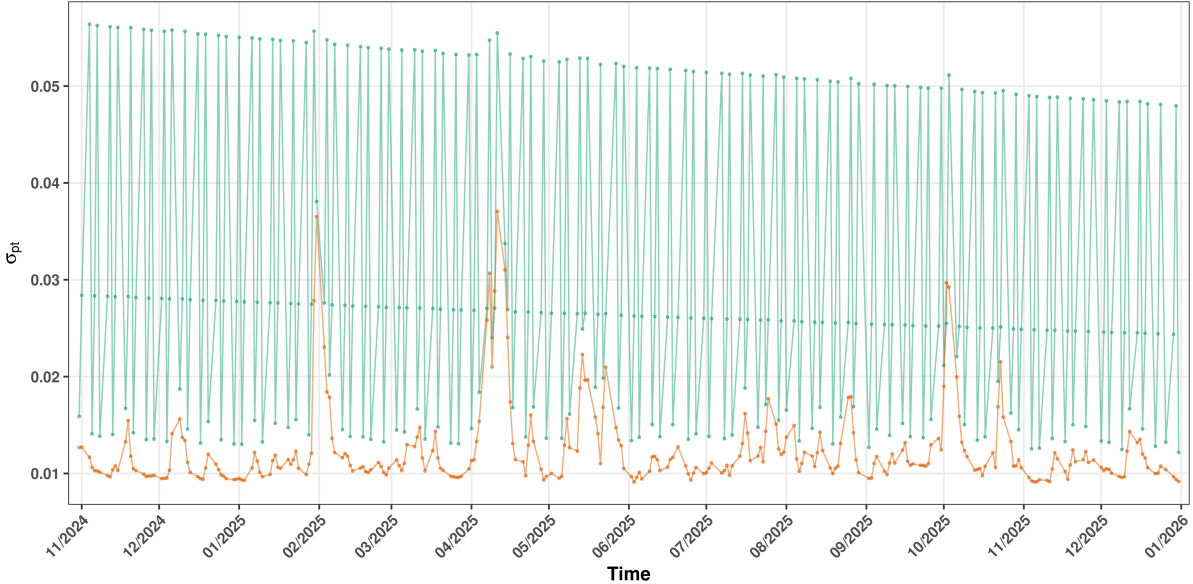


Figure 25: Out-of-sample volatility trajectories estimated by the univariate GARCH model (green) and the DCC-GARCH model (orange) for the optimal portfolio starting from the node “Danaher”.

Figure 25 depicts the out-of-sample volatility trajectories estimated by the univariate GARCH models (green) and the DCC-GARCH model (orange) for the optimal portfolio originating from the node “Danaher.” The figure corroborates the findings from the in-sample analysis (23), showing that the volatility of the optimal portfolio, as estimated by the DCC-GARCH model, is consistently lower and smoother compared to the volatility implied by the virtual portfolio, where univariate GARCH models are applied individually to the constituent assets assumed to be independent. Figure 26 depicts the time-varying correlations ( $\rho_t$ ) estimated for the selected nodes through the DCC-GARCH model over the out-of-sample period. By capturing the evolving negative co-movements among portfolio assets, the BPASGM-based

approach enhances the modeling of systemic risk and asset interdependencies, resulting in a portfolio that exhibits systematically lower volatility both in-sample and out-of-sample.

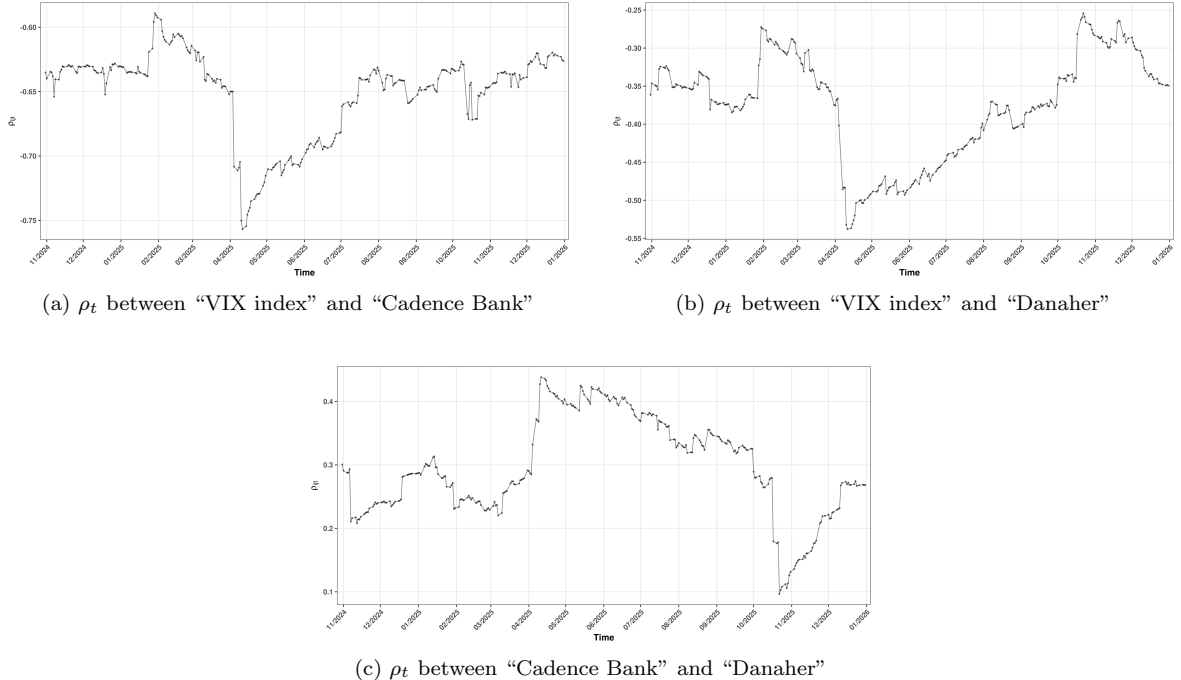


Figure 26: Time-varying conditional correlations  $\rho_t$  (Eq. (23)) estimated via a DCC-GARCH model for out-of-sample period for the optimal portfolio starting from the node "Danaher".

## 6 Conclusions

This paper has introduced the Best-Path Asset Selection Graphical Model (BPASGM), a dependence-aware framework for asset selection and portfolio construction that extends the Best-Path Algorithm from dependency discovery to an operational portfolio methodology. BPASGM integrates sparse graphical modeling with a structured pruning procedure that explicitly accounts for the sign and redundancy of dependence relationships among asset returns.

The proposed method is not intended to improve upon the theoretical mean-variance optimum defined under known population parameters. Rather, it addresses the practical limitations of sample-based mean-variance optimization in high-dimensional settings, where estimation error and redundant dependencies play a dominant role. By conditioning portfolio construction on a carefully selected subset of assets characterized by weak or negative dependence, BPASGM improves robustness and realized performance in finite samples.

Monte Carlo simulations and empirical evidence show that BPASGM-based portfolios exhibit lower realized volatility, improved risk-adjusted performance, and substantial reductions in portfolio cardinality relative to classical sample-based Markowitz portfolios. These improvements reflect both reduced estimation error and the economically motivated selection of assets with favorable dependence structures, rather than a violation of the theoretical risk-return trade-off.

From a methodological perspective, BPASGM represents a significant extension of the original BPA. While BPA focuses on uncovering dependency structures, BPASGM transforms this information into a reproducible asset-selection and portfolio-construction pipeline. The framework is computationally efficient, interpretable, and flexible, and it can be naturally combined with alternative risk measures beyond variance.

Overall, BPASGM provides a bridge between sparse graphical modeling and portfolio theory and offers a promising foundation for future research on dependence-aware asset selection, robust portfolio optimization, and high-dimensional financial decision-making.

## References

T. Aste and T. Di Matteo. Sparse causality network retrieval from short time series. *Complexity*, 2017 (1):4518429, 2017.

T. Aste, W. Shaw, and T. Di Matteo. Correlation structure and dynamics in volatile markets. *New Journal of Physics*, 12(8):085009, 2010.

C. R. Bacon. *Practical risk-adjusted performance measurement*. John Wiley & Sons, 2021.

C. R. Bacon. *Practical portfolio performance measurement and attribution*. John Wiley & Sons, 2023.

W. Barfuss, G. P. Massara, T. Di Matteo, and T. Aste. Parsimonious modeling with information filtering networks. *Physical Review E*, 94(6):062306, 2016.

F. Black and R. Litterman. Global portfolio optimization. *Financial analysts journal*, 48(5):28–43, 1992.

S. Bleik. Concept graphs: Applications to biomedical text categorization and concept extraction. 2013.

F. E. Block. A study of the price to book relationship. *Financial Analysts Journal*, 51(1):63–73, 1995.

T. Bodnar, Y. Okhrin, and N. Parolya. Optimal shrinkage-based portfolio selection in high dimensions. *Journal of Business & Economic Statistics*, 41(1):140–156, 2022.

T. Bollerslev. Generalized autoregressive conditional heteroskedasticity. *Journal of econometrics*, 31(3):307–327, 1986.

M. D. Braga, L. Riso, and M. G. Zoia. The theoretical properties of novel risk-based asset allocation strategies using portfolio volatility and kurtosis. *International Review of Financial Analysis*, page 104728, 2025.

M. Broadie. Computing efficient frontiers using estimated parameters. *Annals of operations research*, 45 (1):21–58, 1993.

D. B. Brown and J. E. Smith. Dynamic portfolio optimization with transaction costs: Heuristics and dual bounds. *Management Science*, 57(10):1752–1770, 2011.

R. Campbell, R. Huisman, and K. Koedijk. Optimal portfolio selection in a value-at-risk framework. *Journal of Banking & Finance*, 25(9):1789–1804, 2001.

R. Carroll, T. Conlon, J. Cotter, and E. Salvador. Asset allocation with correlation: A composite trade-off. *European Journal of Operational Research*, 262(3):1164–1180, 2017.

Y. Choueifaty, T. Froidure, and J. Reynier. Properties of the most diversified portfolio. *Journal of investment strategies*, 2(2):49–70, 2013.

A. Dembo, T. M. Cover, J. A. Thomas, et al. Information theoretic inequalities. *IEEE Transactions on Information theory*, 37(6):1501–1518, 1991.

D. Edwards, G. C. De Abreu, and R. Labouriau. Selecting high-dimensional mixed graphical models using minimal aic or bic forests. *BMC bioinformatics*, 11(1):18, 2010.

R. Engle. Dynamic conditional correlation: A simple class of multivariate generalized autoregressive conditional heteroskedasticity models. *Journal of business & economic statistics*, 20(3):339–350, 2002.

N. Eshima and M. Tabata. Entropy correlation coefficient for measuring predictive power of generalized linear models. *Statistics & probability letters*, 77(6):588–593, 2007.

N. Eshima and M. Tabata. Entropy coefficient of determination for generalized linear models. *Computational statistics & data analysis*, 54(5):1381–1389, 2010.

F. J. Fabozzi, H. M. Markowitz, and F. Gupta. Portfolio selection. *Handbook of finance*, 2:3–13, 2008.

J. Friedman, T. Hastie, and R. Tibshirani. Sparse inverse covariance estimation with the graphical lasso. *Biostatistics*, 9(3):432–441, 2008.

L. Gan, N. N. Narisetty, and F. Liang. Bayesian regularization for graphical models with unequal shrinkage. *Journal of the American Statistical Association*, 114(527):1218–1231, 2019.

A. Garcia-Bernabeu, A. Hilario-Caballero, F. Tardella, and D. Pla-Santamaria. Esg integration in portfolio selection: A robust preference-based multicriteria approach. *Operations Research Perspectives*, 12:100305, 2024.

C. Gregory, K. Darby-Dowman, and G. Mitra. Robust optimization and portfolio selection: The cost of robustness. *European Journal of Operational Research*, 212(2):417–428, 2011.

J. Hakem. *Enhancing portfolio efficiency: funds separation in markowitz optimization models*. PhD thesis, Vilniaus universitetas., 2025.

R. A. Horn and C. R. Johnson. *Matrix analysis*. Cambridge university press, 2012.

H. Jacobs, S. Müller, and M. Weber. How should individual investors diversify? an empirical evaluation of alternative asset allocation policies. *Journal of Financial Markets*, 19:62–85, 2014.

M. I. Jordan et al. Graphical models. *Statistical science*, 19(1):140–155, 2004.

A. Kraskov, H. Stögbauer, and P. Grassberger. Estimating mutual information. *Physical review E*, 69(6):066138, 2004.

N. Lassance and F. Vrins. Portfolio selection: A target-distribution approach. *European Journal of Operational Research*, 310(1):302–314, 2023.

S. L. Lauritzen and N. Wermuth. Graphical models for associations between variables, some of which are qualitative and some quantitative. *The annals of Statistics*, pages 31–57, 1989.

O. Ledoit and M. Wolf. Honey, i shrunk the sample covariance matrix. 2003a.

O. Ledoit and M. Wolf. Improved estimation of the covariance matrix of stock returns with an application to portfolio selection. *Journal of empirical finance*, 10(5):603–621, 2003b.

W. Lefebvre, G. Loeper, and H. Pham. Mean-variance portfolio selection with tracking error penalization. *Mathematics*, 8(11):1915, 2020.

R. N. Mantegna. Hierarchical structure in financial markets. *The European Physical Journal B-Condensed Matter and Complex Systems*, 11(1):193–197, 1999.

A. B. Manual. An introduction to statistical learning with applications in r. 2013.

H. Markowitz. Portfolio selection. *The Journal of Finance*, 7(1):77–91, 1952a. ISSN 00221082, 15406261. URL <http://www.jstor.org/stable/2975974>.

H. Markowitz. Portfolio selection/h. markovitz. *The Journal of Finance*, 7(1):77–91, 1952b.

H. M. Markowitz, F. Schirripa, and N. D. Tecotzky. A more efficient frontier. *Journal of Portfolio Management*, page 99, 1999.

R. D. Martin, A. Clark, and C. G. Green. Robust portfolio construction. In *Handbook of portfolio construction*, pages 337–380. Springer, 2010.

M. J. Mauboussin. What does an ev/ebitda multiple mean. *Bluemont Investment Research*, pages 1–19, 2018.

N. Meinshausen and P. Bühlmann. High-dimensional graphs and variable selection with the lasso. 2006.

A. Meucci. Managing diversification. *Risk*, pages 74–79, 2009.

R. O. Michaud and R. Michaud. Estimation error and portfolio optimization: a resampling solution. Available at SSRN 2658657, 2007.

P. M. Mirete-Ferrer, A. Garcia-Garcia, J. S. Baixauli-Soler, and M. A. Prats. A review on machine learning for asset management. *Risks*, 10(4):84, 2022.

L. Müller and M. Joubrel. A novel approach to sustainable mean-variance portfolio optimization: Accounting for esg-related uncertainty. *Finance Research Letters*, page 108056, 2025.

N. Musmeci, T. Aste, and T. Di Matteo. Risk diversification: a study of persistence with a filtered correlation-network approach. *arXiv preprint arXiv:1410.5621*, 2014.

A. Nezlobin, M. V. Rajan, and S. Reichelstein. Structural properties of the price-to-earnings and price-to-book ratios. *Review of Accounting Studies*, 21(2):438–472, 2016.

L. Olbert. Financial analysts’ use of industry specific stock valuation models. *Journal of Applied Accounting Research*, 26(6):108–138, 2025.

J. Olmo. Estimation error in optimal portfolio allocation problems. In *Oxford Research Encyclopedia of Economics and Finance*. 2023.

Z. Pan and L. Liu. Forecasting stock return volatility: A comparison between the roles of short-term and long-term leverage effects. *Physica A: Statistical Mechanics and its Applications*, 492:168–180, 2018.

M. D. Patil and S. S. Sane. Dimension reduction: A review. *International Journal of Computer Applications* 92, 16:23–29, 2014.

G. Peralta and A. Zareei. A network approach to portfolio selection. *Journal of Empirical Finance*, 38: 157–180, 2016.

F. Pozzi, T. Di Matteo, and T. Aste. Centrality and peripherality in filtered graphs from dynamical financial correlations. *Advances in Complex Systems*, 11(06):927–950, 2008.

F. Pozzi, T. Di Matteo, and T. Aste. Spread of risk across financial markets: better to invest in the peripheries. *Scientific reports*, 3(1):1665, 2013.

M. Raddant and T. Di Matteo. A look at financial dependencies by means of econophysics and financial economics. *Journal of Economic Interaction and Coordination*, 18(4):701–734, 2023.

A. H. Ramadan. *Determinants of capital structure and the firm’s financial performance: An application on the UK capital market*. University of Surrey (United Kingdom), 2009.

R. Riccobello, G. Bonaccolto, P. J. Kremer, S. Paterlini, and M. Bogdan. Sparse graphical modelling for minimum variance portfolios. Available at SSRN 4383314, 2023.

L. Riso and M. Guerzoni. Concept drift estimation with graphical models. *Information Sciences*, 606: 786–804, 2022.

L. Riso, M. G. Zoia, and C. R. Nava. Feature selection based on the best-path algorithm in high dimensional graphical models. *Information Sciences*, 649:119601, 2023.

K. Sadeghi and S. Lauritzen. Markov properties for mixed graphs. 2014.

K. Scheinberg, S. Ma, and D. Goldfarb. Sparse inverse covariance selection via alternating linearization methods. *Advances in neural information processing systems*, 23, 2010.

W. F. Sharpe. The sharpe ratio. *Journal of portfolio management*, 21(1):49–58, 1994.

F. A. Sortino and S. Satchell. *Managing downside risk in financial markets*. Butterworth-Heinemann, 2001.

X. Tu and B. Li. Robust portfolio selection with smart return prediction. *Economic Modelling*, 135: 106719, 2024.

H. R. D. Vinod and D. Reagle. *Preparing for the worst: Incorporating downside risk in stock market investments*. John Wiley & Sons, 2004.

R. E. Whaley. The investor fear gauge. *Journal of portfolio management*, 26(3):12, 2000.

J. Yin and H. Li. A sparse conditional gaussian graphical model for analysis of genetical genomics data. *The annals of applied statistics*, 5(4):2630, 2011.

T. Zerenner, P. Friederichs, K. Lehnertz, and A. Hense. A gaussian graphical model approach to climate networks. *Chaos: An Interdisciplinary Journal of Nonlinear Science*, 24(2), 2014.

Q. Zhou. Portfolio optimization with robust covariance and conditional value-at-risk constraints. *arXiv preprint arXiv:2406.00610*, 2024.

## A Best Path Algorithm

The BPA performs variable selection by leveraging the structure of the HDGM [see, among others, [Edwards et al., 2010](#), [Riso and Guerzoni, 2022](#)], exploiting mutual information to define the topology of the resulting tree or forest. As commonly acknowledged, Mutual Information (MI) [[Kraskov et al., 2004](#)] quantifies the information gain in one variable resulting from the reduction of its entropy when the latter is explained by another variable. Therefore, the greater MI between two variables, the more significant the explanatory role that one variable may have for the other. The algorithm identifies the set of admissible predictors for  $X_i$  by measuring MI between the variables in the graph that belong to different path steps  $ps_i$  connecting them to  $X_i$ . A path step is a collection of variables linked with the target variable  $X_i$ . Path steps are ranked based on the (maximum) distance of the variables from  $X_i$ . The best path-step is the one including variables that share the greatest MI with  $X_i$ , that is

$$MI(X_i, \mathbf{X}_{ps_i}) \geq MI(X_i, \mathbf{X}_{ps_j}), i \neq j, i = 1, \dots, p \quad (\text{A.1})$$

where  $\mathbf{X}_{ps_i}$ ,  $\mathbf{X}_{ps_j}$  denote the set of variables belonging to the path-steps  $ps_i$  and  $ps_j$ . The MI between  $X_i$  and the variables belonging to different path-steps is then quantified using the Kullback-Leibler Information ( $KL$ ) index. The  $KL$  index measures the divergence between the probability densities of two random variables and is connected to their MI, as the latter corresponds to the expectation of  $KL$  between their densities [[Dembo et al., 1991](#)].

In the BPA, MI between  $X_i$  and the variables of a given path-step, say  $\mathbf{X}_{ps_i}$ , is evaluated by measuring the divergence between the distribution of  $X_i$  and that of its projection onto the space generated by  $\mathbf{X}_{ps_i}$ , denoted as  $f(X_i|\mathbf{X}_{ps_i})$ , that is:

$$MI(X_i, \mathbf{X}_{ps_i}) = \mathbb{E}_{f(X_i)}[KL^{(s)}(f(X_i), f(X_i|\mathbf{X}_{ps_i}))]. \quad (\text{A.2})$$

where  $KL^{(s)}$  is the symmetric KL Information, defined as follows

$$KL^{(s)}[f(X_i), f(X_i|\mathbf{X}_{ps_i})] = KL[f(X_i), f(X_i|\mathbf{X}_{ps_i})] + KL[f(X_i|\mathbf{X}_{ps_i}), f(X_i)] \quad (\text{A.3})$$

$KL^{(s)}$  is linked to the entropy coefficient (EC) via the following relationship

$$EC(X_i, \mathbf{X}_{ps_i}) = \frac{1}{\#\{X_j \in ps_i\}} \sum_{X_j \in ps_i} KL^{(s)}[f(X_i), f(X_i|\mathbf{X}_{ps_i})] \quad (\text{A.4})$$

and in turn to the entropy coefficient of determination specified as [[Eshima and Tabata \[2007, 2010\]](#)])

$$ECD = \frac{EC}{EC + 1} \quad (\text{A.5})$$

The ECD index is a generalization of the standard coefficient of determination and it can be viewed as the proportion of the variance/entropy of  $X_i$ , explained by  $\mathbf{X}_{ps_i}$ .

Once, the set of best predictors for the variable  $X_i$  is detected, the explanatory role of each of them is investigated by applying the [Kraskov et al. \[2004\]](#) test. This test checks if a relationships exists between  $X_i$  and each variable of the optimal pat-step  $X_i$ . If some variables within  $ps_i$  are not statistically significant for  $X_i$ , the set of predictors can be further reduced by ruling out them. This procedure leads to a more parsimonious set of predictors for  $X_i$ .

For the best optimal set  $\mathbf{X}_{ps_i}$  of predictors for  $X_i$  detected via the BPA, a relationship like the following can be assumed to hold

$$X_i \approx \phi(\mathbf{X}_{ps_i}) + \epsilon$$

where  $\phi(\cdot)$  is a generic function belonging to the family of the generalized linear models (GLMs) [[Eshima and Tabata, 2007](#)], and  $\epsilon$  is a stochastic term.

## B Constituent assets in the returns dataset

Table 2: Codes of the assets (including stocks and exchange rates) used to label nodes in the analysis

Label	Returns Name	Label	Returns Name	Label	Returns Name	Label	Returns Name
1	Microsoft	91	Paychex	181	Loews	271	Comerica
2	Apple	92	Csx	182	Gen Digital	272	Toro
3	Berkshire Hathaway A	93	Public Storage	183	Southwest Airlines	273	Spx Technologies
4	Walmart	94	Fedex	184	Halliburton	274	Repigen
5	Jp Morgan Chase Co	95	Oneok	185	Keycorp	275	Light Wonder
6	Eli Lilly	96	Truist Financial	186	Carlisle Cos	276	Zions Bancorp
7	Exxon Mobil	97	Fair Isaac	187	Caseys General Stores	277	Rli
8	Oracle	98	Norfolk Southern	188	Clorox	278	Lattice Semiconductor
9	Johnson Johnson	99	Ww Grainger	189	Snapon	279	Badger Meter
10	Procter Gamble	100	Becton Dickinson	190	Cooper Cos	280	Slm
11	Home Depot	101	Paccar	191	Brownforman B	281	Idacorp
12	Unitedhealth Group	102	Kroger	192	Genuine Parts	282	Biorad Laboratories A
13	Bank Of America	103	American Intlgp	193	Alliant Energy	283	Bath And Body Works
14	Coca Cola	104	Schlumberger	194	Baxter Intl	284	Hf Sinclair
15	Chevron	105	Dominion Energy	195	Western Digital	285	Synovus Financial
16	Wells Fargo Co	106	Ross Stores	196	Evergy	286	Alaska Air Group
17	Abbott Laboratories	107	Exelon	197	West Pharmsvs	287	Louisiana Pacific
18	International Busmchs	108	Fastenal	198	Omnicon Group	288	Arrow Electronics
19	Ge Aerospace	109	Kimberlyclark	199	Jacobs Solutions	289	Brinker Intl
20	Mcdonalds	110	Target	200	Best Buy	290	Apa
21	Att	111	Cummins	201	Curtiss Wright	291	Ryder System
22	American Express	112	Occidental Ptl	202	Ball	292	Newmarket
23	Merck Company	113	Ford Motor	203	Unum Group	293	Oshkosh
24	Walt Disney	114	L3harris Technologies	204	Udr	294	Kirby
25	Verizon Communications	115	Hess	205	Graco	295	Lincoln National
26	Pepsico	116	Xcel Energy	206	Idex	296	Dillards A
27	Rtx	117	Electronic Arts	207	Tenet Healthcare	297	Cadence Bank
28	Progressive Ohio	118	Ametek	208	Avery Dennison	298	Moog A
29	Advanced Micro Devices	119	Pubserentergp	209	Hunt Jb Transport Svs	299	Mattel
30	Adobe	120	Consolidated Edison	210	Jack Henry And Associates	300	Teleflex
31	Texas Instruments	121	Corning	211	Cna Financial	301	Interdigital
32	Sp Global	122	Valero Energy	212	Masco	302	Federal Signal
33	Charles Schwab	123	Pge	213	Textron	303	Selective Ingp
34	Caterpillar	124	Baker Hughes A	214	Teradyne	304	Southwest Gas Holdings
35	Thermo Fisher Scientific	125	Entergy	215	Royal Gold	305	Balchem
36	Boeing	126	Vulcan Materials	216	Healthpeak Properties	306	United States Cellular
37	Stryker	127	Cardinal Health	217	Clean Harbors	307	Cirrus Logic
38	Nextera Energy	128	Hershey	218	J M Smucker	308	Gatx
39	Tjx	129	Wec Energy Group	219	Encompass Health	309	Commercial Mtls
40	Amgen	130	Sysco	220	Mastec	310	V F
41	Honeywell Intl	131	Constellation Brands A	221	Universal Health Svsb	311	Champion Homes
42	Danaher	132	Equifax	222	Crown Hdg	312	United Bankshares
43	Deere	133	Eqt	223	Essential Utilities	313	Coeur Mining
44	Citigroup	134	Rockwell Automation	224	Leonardo Drs	314	Gentex
45	Union Pacific	135	Heico	225	Conagra Brands	315	Modine Manufacturing
46	Comcast A	136	Humana	226	Franklin Resources	316	Cognex
47	Pfizer	137	Texas Pacific Land Trust	227	Coherent	317	Fnb
48	Applied Mats	138	General Mills	228	Nordson	318	Txnm Energy
49	Automatic Data Proc	139	Raymond James Finl	229	Pinnacle West Cap	319	Meritage Homes
50	Lowes Companies	140	Kellanova	230	Service Corpintl	320	Timken
51	Conocophillips	141	Lennar A A	231	Revity	321	Icahn Enterprises
52	Marsh Mcleman	142	Mt Bank	232	Carpenter Tech	322	New Jersey Res
53	Analog Devices	143	Dte Energy	233	The Campbell S Company	323	Cousins Props
54	Fiserv	144	W R Berkley	234	Molson Coors Beverage (B)	324	White Mountains Ingp
55	Altria Group	145	Rollins	235	Jefferies Financial Group	325	Fmc
56	Southern	146	State Street	236	Viatris	326	Lancaster Colony
57	Lam Research	147	Nucor	237	Toll Brothers	327	Robert Half
58	Micron Technology	148	Ameren	238	American Finlgpholio	328	Allianceberstein Hldg Unt
59	Bristol Myers Squibb	149	Ppl	239	Sei Investments	329	Lumen Technologies
60	Waste Management	150	Carnival	240	Ati	330	Sealed Air
61	Intel	151	First Ctznbcscha	241	Globe Life	331	Whirlpool
62	Kla	152	Atmos Energy	242	Coca Cola Consolidated	332	Sonoco Products
63	Cigna	153	Hp	243	Smith	333	Spire
64	Sherwinwilliams	154	Fifth Third Bancorp	244	Stanley Black Decker	334	S&P 500 Composite Price Index
65	Cintas	155	Ppg Industries	245	Stifel Financial	335	Stoxx Europe 600 E Price Index
66	Arthur J Gallagher	156	Firstenergy	246	Interpublic Group	336	Ftse 100 Price Index
67	Nike B	157	Centerpoint En	247	Oge Energy	337	Dax Performance Price Index
68	Cvs Health	158	Tyler Technologies	248	Regal Rexnord	338	Topix Price Index
69	Cadence Design Sys	159	Dover	249	Mgm Resorts Intl	339	Nasdaq Composite Price Index
70	Parkerhannifin	160	Markel Group	250	Eastgroup Props	340	France Cac 40 Price Index
71	3m	161	International Paper	251	New York Times A	341	Ibex 35 Price Index
72	General Dynamics	162	Archer Daniels Midland	252	Hasbro	342	Swiss Market Price Index
73	Colgatepalm	163	Eversource Energy	253	Gap	343	Oslo Exchange
74	Ecolab	164	Cincinnati Finl	254	Commerce Bsch	344	Nikkei 225 Index
75	Illinois Tool Works	165	Church Dwight Co	255	Applied Indltechs	345	Russell 2000 Price Index
76	Williams	166	Huntington Bsch	256	Webster Financial	346	Dow Jones Index
77	Northrop Grumman	167	Cma Energy	257	Chemed	347	Sptsx 60 Index Price Index
78	Motorola Solutions	168	Edison Intl	258	Donaldson Co	348	Nyse Composite Price Index
79	Pnfcnvsrgp	169	Devon Energy	259	Federal Realty Invst	349	Vix Index
80	Us Bancorp	170	Pultegroup	260	Old National Bancorp	350	Usd To Eur Exchange Rate
81	Howmet Aerospace	171	T Rowe Price Group	261	Watts Water Techs	351	Jpy To Usd Exchange Rate
82	Emerson Electric	172	Mccormick Company Nv	262	Nnn Reit	352	Chf To Usd Exchange Rate
83	Autodesk	173	Williams Sonoma	263	Biotechnie	353	Cad To Usd Exchange Rate <sup>6</sup>
84	Travelers Cos	174	Tyson Foods A	264	Umb Financial	354	Us To Uk Gbp Exchange Rate
85	Eog Res	175	Ptc	265	Hr Block	355	Cad To Usd Exchange Rate <sup>7</sup>
86	Air Prds Chems	176	Northern Trust	266	Fannie Mae	356	Usd To Aud Exchange Rate
87	Newmont	177	Regions Finlnew	267	Ugi	357	Hkd To Usd Exchange Rate
88	Monster Beverage	178	Weyerhaeuser	268	Vornado Realty Trust	358	SEK To Usd Exchange Rate
89	Aflac	179	Intlfavors Frag	269	Middleby		
90	Amerelecprw	180	Nisource	270	National Fuel Gas		

## C Proof of Lemma 2.1

*Proof.* Let  $X = \{X_1, \dots, X_p\}$  denote the set of asset return variables, and let  $X_{ps_i} \subset X \setminus \{X_i\}$  denote the optimal predictor set of  $X_i$  selected by the Best-Path Algorithm (BPA). By construction, BPA selects  $X_{ps_i}$  as the subset of variables that maximizes the explanatory information for  $X_i$  according to an information-theoretic criterion.

This selection can be equivalently interpreted as choosing  $X_{ps_i}$  such that the conditional mutual information between  $X_i$  and any additional variable outside  $X_{ps_i}$ , given  $X_{ps_i}$ , is negligible. Formally, for any  $Z \subseteq X \setminus X_{ps_i}$ , BPA ensures that

$$I(X_i; Z | X_{ps_i}) \approx 0,$$

in the sense that including variables in  $Z$  does not provide a meaningful increase in explanatory power for  $X_i$  beyond that already captured by  $X_{ps_i}$ .

Using the chain rule for mutual information, we can decompose the mutual information between  $X_i$  and the entire set of remaining variables as

$$I(X_i; X \setminus \{X_i\}) = I(X_i; X_{ps_i}) + I(X_i; X \setminus X_{ps_i} | X_{ps_i}).$$

Since BPA selects  $X_{ps_i}$  to capture essentially all the information about  $X_i$  contained in  $X \setminus \{X_i\}$ , the second term in the decomposition must be approximately zero. Hence,

$$I(X_i; X \setminus X_{ps_i} | X_{ps_i}) \approx 0.$$

Vanishing (or approximately vanishing) conditional mutual information is equivalent to (approximate) conditional independence. Therefore, the BPASGM construction implies the conditional independence property

$$X_i \perp\!\!\!\perp X \setminus X_{ps_i} | X_{ps_i},$$

which establishes the stated result.  $\square$

This conditional independence is a structural property induced by the BPA selection mechanism and does not rely on assumptions of statistical consistency, causal sufficiency, or recovery of a true Markov blanket.

## D Data Generating Process

The data-generating process is articulated into two main steps.

The first six return series ( $R_1$  to  $R_6$ ) are generated using a combination of stochastic noise, autoregressive dynamics, and nonlinear transformations. Specifically, the true mean ( $\mu_i$ ) and standard deviation ( $\sigma_i$ ) for each asset  $i \in \{1, \dots, 6\}$  are independently sampled from uniform distributions over the intervals  $[0.0001, 0.0009]$  and  $[0.0003, 0.08]$ , respectively.

To capture temporal dependence, the noise-generating function is defined as:

$$\text{gen\_noise}(\mu, \sigma) = \text{AR}(1) \text{ process with } \phi = 0.2 \text{ and innovation standard deviation } \sigma + \mu.$$

The first six return series are then constructed as follows:

$$\begin{aligned} R_1 &= \mathcal{N}(\mu_1, \sigma_1^2) + \text{gen\_noise}(0, \sigma_1), \\ R_2 &= \mathcal{N}(\mu_2, \sigma_2^2) + \text{gen\_noise}(0, \sigma_2), \\ R_3 &= -0.003 \cdot \exp(-|R_1|) + 0.5R_2 + \mathcal{N}(\mu_3, \sigma_3^2) + \text{gen\_noise}(0, \sigma_3), \\ R_4 &= -0.9R_1 + \mathcal{N}(\mu_4, \sigma_4^2) + \text{gen\_noise}(0, \sigma_4), \\ R_5 &= 0.6R_4 - 0.5R_2 + \mathcal{N}(\mu_5, \sigma_5^2) + \text{gen\_noise}(0, \sigma_5), \\ R_6 &= \tanh(0.8R_3 - 0.5R_5) + \mathcal{N}(\mu_6, \sigma_6^2) + \text{gen\_noise}(0, \sigma_6). \end{aligned}$$

The remaining six return series ( $R_7$  to  $R_{12}$ ) are generated as nonlinear and linear transformations of the first six, thereby introducing more intricate dependency patterns. For these assets, the means and standard deviations are drawn from the intervals  $[0.0001, 0.001]$  and  $[0.006, 0.016]$ , respectively.

The definitions of these series are as follows:

$$\begin{aligned}
R_7 &= -0.9R_5 - 0.6R_4 + \text{gen\_noise}(\mu_7, \sigma_7), \\
R_8 &= -0.8R_7 - 0.4R_3 + \text{gen\_noise}(\mu_8, \sigma_8), \\
R_9 &= 0.3R_3 + \text{gen\_noise}(\mu_9, \sigma_9), \\
R_{10} &= \log(1 + |R_1 + R_5|) + 0.2R_9 + \text{gen\_noise}(\mu_{10}, \sigma_{10}), \\
R_{11} &= 0.2R_8 + \max(R_2, R_1) + \text{gen\_noise}(\mu_{11}, \sigma_{11}), \\
R_{12} &= -0.6R_4 - 0.4R_6 + \text{gen\_noise}(\mu_{12}, \sigma_{12}).
\end{aligned}$$

The simulated dataset ( $\mathbf{X}_{\text{simulated}}$ ) captures realistic interdependencies among asset returns, including non-reciprocal effects, nonlinear interactions, and overlapping informational content. This level of complexity makes it particularly well suited for evaluating the ability of the BPASGM algorithm to recover relevant dependencies and to select optimal asset subsets under conditions that closely resemble real-world financial data. Such an experimental design provides a rigorous basis for assessing the algorithm's feature selection performance in environments characterized by intricate structural relationships [Riso et al., 2023].

## E Comparison performance with GLASSO

In this section, we present a comparative performance analysis between the proposed BPASGM algorithm and the Graphical Lasso (GLASSO) method introduced by Friedman et al. [2008]. The GLASSO is a penalized likelihood approach for estimating a sparse precision matrix (the inverse of the covariance matrix) for continuous variables by applying an  $\ell_1$  regularization term that induces sparsity in the estimated inverse covariance structure.

Let  $R \in \mathbb{R}^{T \times N}$  denote the matrix of centered asset returns. The GLASSO optimization problem is formulated as

$$\hat{\Theta} = \arg \max_{\Theta \succ 0} \left\{ \log \det \Theta - \text{tr}(S\Theta) - \lambda \sum_{i \neq j} |\theta_{ij}| \right\},$$

where  $S = \frac{1}{T} R^\top R$  denotes the sample covariance matrix,  $\Theta = \Sigma^{-1}$  is the precision matrix, and  $\lambda \geq 0$  controls the degree of sparsity. Non-zero entries in  $\hat{\Theta}$  correspond to conditional dependencies between pairs of assets, capturing partial correlations conditional on all others. Higher values of  $\lambda$  yield sparser dependence structures, whereas lower values result in denser interconnections. The selection of an appropriate regularization level has been extensively discussed in the literature [see, among others, Yin and Li, 2011, Friedman et al., 2008, Pozzi et al., 2013, 2008]. In this study, rather than fixing a single optimal parameter, we examine the entire range of possible regularization levels to benchmark the performance of BPASGM against the set of portfolios implied by GLASSO under varying degrees of sparsity.

For each value of  $\lambda$ , the precision matrix  $\hat{\Theta}^{(\lambda)}$  is computed and subsequently binarized to identify statistically significant conditional dependencies. Each element  $\hat{\theta}_{ij}^{(\lambda)}$  reflects the conditional relationship between assets  $i$  and  $j$ ; retaining only the most relevant connections, the adjacency matrix  $A^{(\lambda)}$  is defined as:

$$A_{ij}^{(\lambda)} = \begin{cases} 1, & \text{if } |\hat{\theta}_{ij}^{(\lambda)}| > \tau, \\ 0, & \text{otherwise,} \end{cases} \quad A_{ii}^{(\lambda)} = 0,$$

where  $\tau > 0$  determines the minimum magnitude of a conditional dependency to be considered economically meaningful. The matrix  $A^{(\lambda)}$  defines an undirected network  $G^{(\lambda)} = (V, E^{(\lambda)})$ , whose nodes correspond to assets and edges represent significant conditional relations.

On each network, standard centrality measures are computed to quantify the structural relevance of individual assets. The degree centrality of node  $i$  is given by

$$\deg(i) = \sum_{j=1}^p A_{ij},$$

and reflects its direct level of interconnectedness. The betweenness centrality,

$$\text{betw}(i) = \sum_{s \neq i \neq t} \frac{\sigma_{st}(i)}{\sigma_{st}},$$

measures how frequently node  $i$  lies on the shortest paths connecting other nodes, where  $\sigma_{st}$  is the number of shortest paths between nodes  $s$  and  $t$ , and  $\sigma_{st}(i)$  denotes those passing through  $i$ . Finally, the closeness centrality captures the average geodesic proximity of an asset to all others:

$$\text{clos}(i) = \frac{1}{\sum_{j=1}^p d(i, j)},$$

where  $d(i, j)$  is the shortest-path distance between assets  $i$  and  $j$ .

Assets are retained for portfolio construction if they are either directly connected or occupy a central position in the conditional dependency network. Formally, the selected subset of assets  $S$  is given by:

$$S = \{ i \in V : \deg(i) > 0 \text{ or } \text{betw}(i) > \text{median}(\text{betw}) \text{ or } \text{clos}(i) > \text{median}(\text{clos}) \}.$$

This network-based filtering identifies assets that play a key structural role in the system of conditional dependencies, providing an economically interpretable and data-driven reduction of the investment universe prior to optimization. By combining sparse graphical modeling [Friedman et al., 2008] with network-theoretic filtering [Mantegna, 1999, Peralta and Zareei, 2016], this approach integrates statistical regularization with topological structure to extract the most informative subset of assets for allocation.

By iterating this selection procedure over the full range of  $\lambda$  values and computing the corresponding Sharpe and Sortino ratios for each resulting minimum-variance portfolio, we obtained a detailed performance mapping as a function of network sparsity. Figures 27 illustrate that the portfolios selected by BPASGM consistently outperform those derived from the GLASSO approach across all sparsity levels. Specifically, both the annualized Sharpe ratio (Figure 27a) and the annualized Sortino ratio (Figure 27b) of BPASGM-based portfolios (orange line) surpass those of GLASSO-based portfolios (green line), confirming the superior robustness and efficiency of the proposed method.

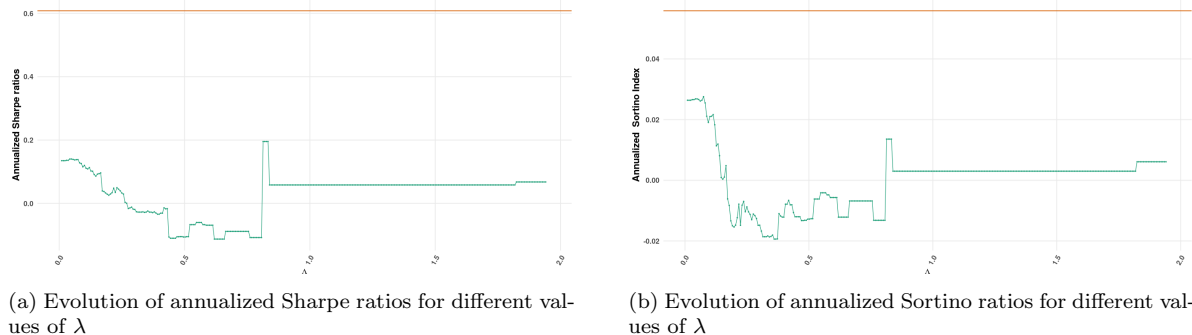


Figure 27: Annualized Sharpe ratios (panel (a)) and annualized Sortino ratios (panel (b)) for different values of  $\lambda$  (green line). The corresponding performance of the optimal portfolio selected via BPASGM is shown in orange.